Ecological Informatics 31 (2016) 1–17

Contents lists available at ScienceDirect

Ecological Informatics

journal homepage: www.elsevier.com/locate/ecolinf

Optimizing the complexity of phytoplankton functional group modeling: An allometric approach

Yuko Shimoda [a], Yerubandi R. Rao [b], Sue Watson [b], George B. Arhonditsis [a,*]

[a] Department of Physical & Environmental Sciences, University of Toronto, Toronto, ON M1C 1A4, Canada
[b] Environment Canada, Water Science and Technology, National Water Research Institute, Burlington, ON L7R 4A6, Canada

ARTICLE INFO

Article history:
Received 24 August 2015
Received in revised form 16 October 2015
Accepted 3 November 2015
Available online 11 November 2015

Keywords:
Complex mathematical models
Resource competition
Allometric theory
Phytoplankton functional grouping
Ecological diversity

ABSTRACT

Elucidating patterns and mechanisms that shape phytoplankton assemblages is a popular area of research for empirical and theoretical ecologists. Despite the daunting complexity of phytoplankton dynamics, much of our current understanding has been based on simple models describing food-web interactions with few differential equations. Skeptical views in the literature raise concerns about the increasing model complexity and advice to seek parsimony rather than simplicity. To address this controversy (simple versus complex models), we propose the introduction of an extra layer of causality into plankton models by connecting algal processes (maximum growth rates, nutrient kinetics, settling velocities, metabolic rates) with species-specific morphological features (cell volume, surface-to-volume ratio, shape). In this study, we demonstrate the capacity of a size-based plankton model to reproduce observed water quality patterns (phosphate, total phosphorus, nitrate, total ammonia, total nitrogen, chlorophyll *a*, and total zooplankton biomass) in the Hamilton Harbour, Ontario. Consistent with empirical evidence, our modeling analysis showed that small algal species have a distinct competitive advantage in summer epilimnetic environments across the range of cell volume and nutrient loading conditions examined; especially, when they are characterized by higher optimal temperature for growth. Strong top-down pressure mediated by high zooplankton abundance effectively controls the standing biomass of phytoplankton species that can otherwise realize high growth rates under the conditions typically prevailing in the end-of-summer epilimnetic environments (e.g., higher temperature optima, higher tolerance in low water clarity). Under high zooplankton control, the secondary variations of phytoplankton are modulated by the ambient phosphorus levels and the size-based strategies for resources procurement, such as the regulation of nutrient transport kinetics. By contrast, when the summer algal assemblage is released by the zooplankton grazing, the exceedance of critical phytoplankton biomass levels and the likelihood of harmful algal blooms are determined by the multitude of factors that shape inter-specific competition patterns (e.g., relative abundance of competing species, nutrient uptake kinetics). Our study evaluates the strengths and weaknesses of this approach and identifies future directions that would provide operational models founded upon concepts of allometry.

1. Introduction

Mathematical modeling as a tool for shedding light on ecological patterns is subject to the complexity issue, and the development of simplification/aggregation rules that allow extracting the essential ecosystem features is a central problem in the modeling practice (Arhonditsis and Brett, 2004; Chen et al., 2011; Costanza and Sklar, 1985; Levin, 1992). In this context, one of the fundamental decisions is related to the selection of the optimal aggregation level of biological communities. For example, many studies have examined the efficiency of population (e.g., species), community (e.g., genera, taxa), and aggregate (e.g., biomass, primary productivity, nutrient cycling) variables to illuminate different aspects of ecosystem dynamics (Anderson, 2005; Arhonditsis, 2010; Flynn, 2005). Notwithstanding the satisfactory predictability achieved at higher aggregation levels (Scheffer et al., 2003), there are several compelling reasons to opt for a finer resolution of biotic communities, e.g., species populations are more sensitive to external perturbations (episodic meteorological events, nutrient enrichment), can serve as early warning signs of ecosystem regime shifts, and important facets of biogeochemical cycles are intimately linked to specific functional groups (Cottingham and Carpenter, 1998; Flynn, 2005; Zhao et al., 2008a,b). In particular, phytoplankton is often perceived as sentinel organism of aquatic ecosystem functioning that can affect mass/energy fluxes through their metabolic activity (photosynthesis, respiration, nutrient recycling) and physical material translocation (via active cell migration, passive cell advection or sinking) (Moore et al., 2006; Sarmiento et al., 1993). Nonetheless, skeptical viewpoints caution that the delineation of distinct functional groups from fairly

* Corresponding author. Tel.: +1 416 208 4858; fax: +1 416 287 7279.
E-mail address: georgea@utsc.utoronto.ca (G.B. Arhonditsis).

http://dx.doi.org/10.1016/j.ecoinf.2015.11.001
1574-9541/

heterogeneous algal assemblages poses challenging problems with respect to their robust characterization that can be used for predictive purposes in a wide array of spatiotemporal domains (Anderson, 2005).

The essence of the selection of the optimal resolution level in phytoplankton ecology is to phase out the excessive (and oftentimes uninformative) variability by integrating across multi-species population patterns, while maintaining the sensitivity of individual species to external perturbations (Arhonditsis et al., 2007a). Recognizing the trade-off between sensitivity and predictability, Reynolds et al. (2002) argued in favor of classifying species on the basis of their general functional properties, i.e., morphological, physiological, and ecological characteristics. Functional grouping accounts for different adaptive strategies, and recognizes the interplay between external (e.g., climatic conditions, trophic interactions) and internal (e.g., interspecific competition) factors may be an impediment for reliably predicting the expected signals of phytoplankton community (Huisman and Weissing, 1999; Scheffer et al., 2003; Sommer, 1995;). Phytoplankton functional grouping (PFG) has gradually become a popular modeling framework, offering an appealing alternative to address the dysfunctionality of highly aggregated models, such as those of the Nutrient-Phytoplankton-Zooplankton-Detritus family (Le Quere, 2006; Thingstad et al., 2010). While the PFG strategy is promising, the increased model complexity means that the number of parameters that must be specified from the data increases disproportionally with the number of state variables considered (Arhonditsis et al., 2006; Denman, 2003). The ability to set quantitative (or even qualitative) constraints and ensure a realistic/behavioral simulation may be compromised significantly (Van Nes and Scheffer, 2005), and the inadequate model identifiability may undermine the predictive application of PFG constructs relative to simpler models (Anderson, 2005; Mieleitner and Reichert, 2008).

To address the increasingly important identifiability issue with PFG models, we propose to link phytoplankton physiological processes with specific morphological features (i.e., cell volume, surface-to-volume ratio, and shape). Founded upon concepts of allometric theory, our thesis is that the size and shape of organisms strongly influences their physiological rates, such as maximum growth rates, nutrient kinetics, and basal metabolism, and thus influences their responses to external perturbations, interspecific competition, and ultimately composition of algal assemblages (Cyr and Pace, 1993; Peters, 1983). From a technical standpoint, one of the key features of the allometric approach is that the characterization of simulated plankton groups is no longer based on adjustable parameters, often treated as "properties of convenience" for fitting models to the observed data (Poulin and Franks, 2010), but instead their morphological features are designated as common denominator that influences the corresponding physiological rates. While addressing the implications of model complexity through the introduction of an additional layer (empirical allometric equations) may seem somewhat counterintuitive, the basic premise of this approach is that model parametric uncertainty is more effectively delineated; namely, the literature-based ranges typically assigned to the calibration parameters are now replaced by the parameter standard error values and/or the estimates of residual variability of allometric equations. In a broader context, this practice may (in part) address the problem of complex over-parameterized models (Arhonditsis et al., 2007b; Beven, 2006). This approach also offers a different perspective on the optimization of future data collection. Model calibration is not solely perceived as a typical inverse solution exercise, constantly inviting the collection of data on model outputs and subsequently readjusting the parameters to match measurements and predictions (Shimoda and Arhonditsis, 2016; Zhang and Arhonditsis, 2008). We rather argue that the model parameter estimation requires a more robust experimentation focused on the development (or further refinement) of the causal characterization of model parameters. Moreover, depending on the nature of the dataset used for the allometric regression equations (e.g., marine versus freshwater algae), the proposed method allows the potential users to delineate the application domain more easily and determine to what extent a particular model has local or universal use.

Although a number of studies have used allometric scaling to parameterize planktonic ecosystem models (Elliott et al., 2000, 2001; Kerimoglu et al., 2012; Moloney and Field, 1991; Ray et al., 2001; Sin and Wetzel, 2002; Tian et al., 2000; Wirtz, 2013), the majority of these efforts remained in the theoretical realm and applications in the context of operational modeling are limited. To address this gap, the primary purpose of our study is to evaluate a mathematical model that considers two growth-limiting nutrients (nitrogen and phosphorus) and multiple functional phytoplankton and zooplankton groups to reproduce the mechanisms underlying the eutrophication problems in Hamilton Harbour, Ontario, Canada. The characterization of phytoplankton functional groups is based on allometric regression equations that connect their maximum growth rates, nutrient kinetics, settling velocities, and basal metabolism with user-specified morphological features (cell volume, surface-to-volume ratio, shape). After a basic calibration exercise of the mathematical model against the observed water quality patterns of Hamilton Harbour, we present the results of a Monte Carlo analysis to offer insights into the model's capacity to reproduce the dynamics of algal assemblages under a wide range of environmental conditions. Specifically, we address two important questions of theoretical and practical relevance with respect to the present status and future response of the system: What is the role of algal cell size, allometrically-derived phosphorus uptake kinetics, abiotic conditions, inter-specific competition, and zooplankton grazing control on the relative abundance of the phytoplankton functional groups modeled? What is the impact of hypolimnetic phosphate accumulation on the occurrence of non-linear structural shifts in the summer algal assemblage? Our study concludes by evaluating the strengths and weaknesses of the proposed strategy in order to obtain operational models that build upon the fundamental concepts of allometry.

2. Methods

2.1. Case study

Hamilton Harbour, a large embayment located at the western end of Lake Ontario (Fig. 1a), has a long history of eutrophication problems primarily manifested as excessive algal blooms, low water transparency, and low hypolimnetic oxygen concentrations often beginning in early summer (Hiriart-Baer et al., 2009). Since the mid-1980s, when the harbour was identified as one of the 43 Areas of Concern by the Water Quality Board of the International Joint Commission, the Hamilton Harbour Remedial Action Plan was formulated through government, private sector, and community participants to provide the framework for actions aimed at restoring the system. The foundation of the remedial measures originally proposed for restoring the Hamilton Harbour was based on a conceptual model that dissected the eutrophication problems into a sequence of causal linkages, i.e., fish need aquatic plants for shelter and reproduction, aquatic plants need light to grow, light will only penetrate the water column if chlorophyll *a* levels are sufficiently low, low chlorophyll *a* levels are achieved through sufficiently low total phosphorus (TP) concentrations (Charlton, 2001). Based on empirical relationships between water clarity and the maximum depth of colonization of submerged plants (Chambers and Kalff, 1985), it was estimated that the Secchi disk transparency of 3.0 m was expected to provide approximately 170 ha for plant colonization, which was then used to identify a targeted level of external total phosphorus loading (142 kg day^{-1}) and epilimnetic targets of total phosphorus (TP < 17 μg L^{-1}) and chlorophyll *a* (5–10 μg L^{-1}) concentrations (Charlton, 2001). Indeed, the substantial reduction of TP from the sewage effluents of the four wastewater treatment plants (Woodward Ave, Skyway, Dundas, Waterdown; see Fig. 1a) and the steel mills that discharge into the harbour led to a significant

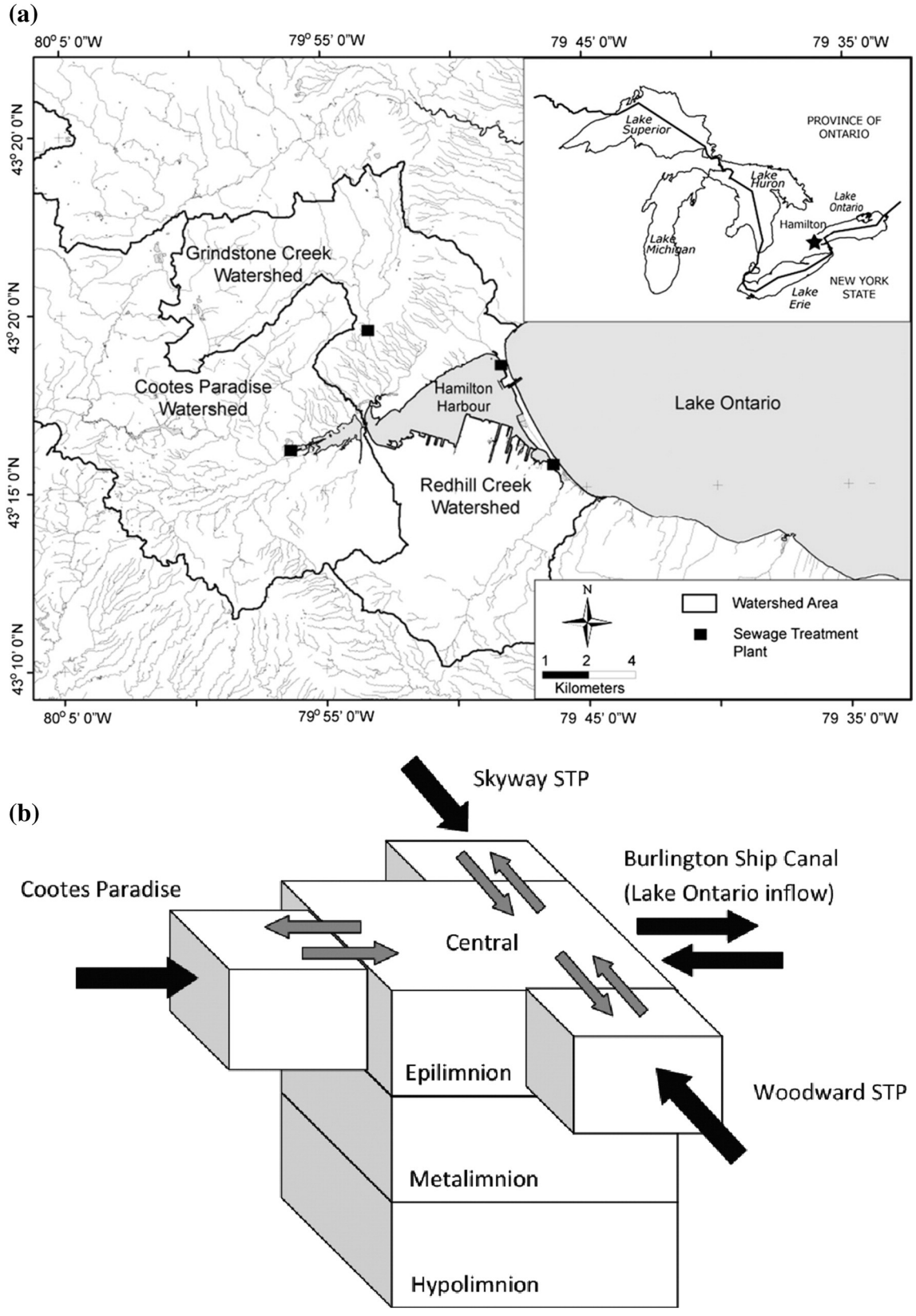

Fig. 1. (a) The Hamilton Harbour, Ontario, Canada; (b) Spatial segmentation of the spatially-explicit model. Black arrows represent loadings/inflows from tributaries into specific spatial segments (Skyway STP, Woodward STP and Cootes Paradise) or exchanges between the harbour and Lake Ontario. Gray shaded arrows represent advective/diffusive mass exchanges among the spatial segments.

decrease in TP concentrations and improved the water clarity, which in turn facilitated aquatic macrophyte resurgence in most areas. However, the system still receives substantial loads of phosphorus (350 kg day^{-1}), ammonia (NH_3) (3,400 kg day^{-1}), and suspended solids (45,000 kg day^{-1}) from the Burlington and Hamilton sewage treatment plants, and therefore only moderate improvements in

epilimnetic TP, chlorophyll a and total ammonia concentrations have been observed since the mid-1990s.

Recent modeling work suggests that the target of chlorophyll *a* concentrations in the Hamilton Harbour lower than 10 μg L^{-1} is attainable, if the Hamilton Harbour RAP TP loading goal of 142 kg day^{-1} is achieved (Gudimov et al., 2010, 2011; Kim et al., 2014; Ramin et al., 2011, 2012). However, the process of setting water quality targets must be pragmatic, and the natural variability should be explicitly accommodated by permitting a realistic frequency of violations, e.g., exceedances of less than 10–15% of the weekly samples during the stratified period should still be considered as compliant. Likewise, the current epilimnetic TP goal of 17 μg L^{-1} is probably too stringent and a somewhat higher value (e.g., 20 μg L^{-1}) may provide a more realistic goal. Two critical aspects of the system dynamics that invite further investigation and will likely determine the success of the restoration efforts are the nutrient recycling mediated by the microbial food web and/or the sediment diagenesis, along with the structural shifts toward a zooplankton community dominated by large-sized and fast-growing herbivores (Gudimov et al., 2011). The latter prospect highlights the notion that the bottom-up (i.e., nutrient loading reduction) approach historically followed in the harbour was sufficient to bring the system in its present state, but any further improvements should be viewed in the context of a combined bottom-up and top-down (i.e., alleviation of the zooplanktivorous pressure) control (Ramin et al., 2011).

2.2. Model description

The Hamilton Harbour model simulates three biogeochemical cycles (i.e., organic carbon, nitrogen, and phosphorus), two zooplankton groups (i.e., omnivorous and herbivorous), and three phytoplankton functional groups. The governing equation for phytoplankton biomass accounts for phytoplankton production and losses due to mortality, settling, dreissenid filtration, and herbivorous zooplankton grazing. The phytoplankton growth is controlled by water temperature as well as nitrogen, phosphorus, and light availability. The three phytoplankton functional groups originally differed with respect to their strategies for resource competition (nitrogen, phosphorus, light, and temperature) and metabolic rates as well as their settling velocities, self-shading effects, and edibility for zooplankton. The functional group A (PFG A)had growth and metabolic attributes of r-selected organisms, superior phosphorus and inferior nitrogen kinetics relative to the rest functional groups, lower tolerance to low light availability, low temperature optima, high sinking velocities, and high palatability as food source for zooplankton. Thus, this functional group was primarily intended to reproduce the dynamics of the spring diatom-dominated phytoplankton community. On the other hand, the functional group PFG C was modeled as a K-strategist in regard to its growth and metabolic properties, a weak phosphorus and dominant nitrogen competitor, with higher tolerance to low light availability, low settling velocities, high temperature optima, and low edibility. The specification of this group aimed to describe the dynamics of the majority of cyanophytes in the harbour. The third group (labeled as PFG B) was parameterized in a way that its average functional properties resembled to those of other major residents of the summer phytoplankton community (chlorophytes, chrysophytes), thereby providing an intermediate competitor that more realistically depicts the continuum between diatom- and cyanobacteria-dominated communities. Detailed description of the original eutrophication model for the Hamilton Harbour was provided in Gudimov et al. (2011), while the associated mathematical formulations are presented in Table 1 of the Electronic Supplementary Material or Table S1. The aforementioned specification of the three active functional groups was revisited with the allometric characterization of their functional properties.

The original model was also based on a three-compartment vertical segmentation representing the epilimnion, mesolimnion, and hypolimnion of the harbour (Gudimov et al., 2010). The depths of the epilimnion and mesolimnion were explicitly specified based on extensive field measurements (1987–2007) and were both set equal to 8 m (Dermott, 2007; Hiriart-Baer et al., 2009). Seasonally-varying mass exchanges among the three compartments were computed using Fick's Law (Hamblin and He, 2003; Klapwijk and Snodgrass, 1985). The exchanges between the Hamilton Harbour and the relatively high quality waters of Lake Ontario through the Burlington Ship Canal were based on the Klapwijk and Snodgrass (1985; see their Fig. 1) conceptual model that postulates 20% of the Lake Ontario inflows to be directly discharged into the epilimnion and mesolimnion, whereas 80% of the fresher oxygenated lake water replaces the hypolimnetic masses in the harbour. In the present study, the spatial segmentation of the aquatic biogeochemical model was upgraded to accommodate the horizontal water quality gradients in the system (Hiriart-Baer et al., 2009). Specifically, we developed a spatially-explicit model that separates the epilimnion into four segments: Cootes Paradise outlet zone, central pelagic zone, and the segments influenced by the Skyway and Woodward wastewater treatment plants (Fig. 1b). While the central zone maintains its original structure with all the basic hydrodynamic patterns (e.g., vertical mixing, exchanges with Lake Ontario), the other three segments represent the shallow regions (<8 m) of the system. The model was forced by the average summer circulation pattern in the harbour, as derived by Rao et al.'s (2009) application of the three-dimensional hydrodynamic model ELCOM (Estuary Lake Coastal Ocean Model). In particular, it was found that the mean surface summer circulation pattern in the Hamilton Harbour is predominantly driven by the frequent westerly

Table 1
Allometric equations used to characterize phytoplankton functional groups with the Hamilton Harbour eutrophication model. In all equations, V and SA/V denote cell volume (μm^3) and surface area to volume ratio (μm^{-1}), respectively.

Size-based parameters	Symbol	Allometric relationship	Unit	SEE	Source
Maximum growth rate	μ_{max}	$\mu_{max} = 10^{0.54}\, V^{-0.15}$	day^{-1}	0.236	1
Maximum growth rate for PFG A	μ_{max}	$\mu_{max} = 10^{0.73}\, V^{-0.17}$	day^{-1}	0.182	1
Basal metabolism	mp	$mp = 0.063–0.008\ \mathrm{Log}\ V$ [a]	day^{-1}	–	2
Half saturation constant for Nitrate uptake	NH	$NH = 10^{-0.71}\, V^{0.52}$	μmol NL^{-1}	0.329	3
Half saturation constant for Phosphorus uptake	KH_p	$KH_p = 10^{-1.5}\, V^{0.53}$	μmol PL^{-1}	0.628	3
Maximum Phosphorus uptake rate	$VP_{maxuptake}$	$VP_{maxuptake} = 10^{-8.4}\, V^{0.81}$	μmol P $cell^{-1}$ day^{-1}	0.537	3
Maximum Phosphorus uptake rate	$VP_{maxuptake}$	$VP_{maxuptake} = 10^{-10.7}\, SA/V^{1.7}$	μg P μm^{-3} h^{-1}	0.165	4
Maximum internal phosphate quota	QP_{max}	$QP_{max} = 10^{-0.29}\, V^{0.767}$	fmol $cell^{-1}$	0.668	5
Minimum internal phosphorus quota	QP_{min}	$QP_{min} = 10^{-1.04}\, V^{0.714}$	fmol $cell^{-1}$	-	5
Settling velocity	u_z	$u_z = 0.029\ C^{0.42}$	m day^{-1}	0.404	6
Light attenuation coefficient for PFGs (Self-shading effect)	$K_{extchla}$	$K_{extchla} = 10^{-x}\, V^{-y}$ [b]	–	–	7
Food quality	$pref_{ZOOP}$	$\mathrm{pref}_{ZOOP} = 1.5–0.3\mathrm{Log}\ V$	–	–	Estimation
Carbon content in cell	C	$C = 10^{-0.665}\, V^{0.939}$	pg C $cell^{-1}$	0.266	8
Carbon content in cell	C	$C = 10^{-0.29}\, V^{0.76}$	pg C $cell^{-1}$	0.200	9

Sources: 1) Tang, 1995; 2) Ray et al., 2001; 3) Edwards et al., 2012; 4) Friebele et al., 1978; 5) Grover, 1989; 6) Moloney and Field, 1991; 7) Fujiki and Taguchi, 2002; 8) Menden-Deuer and Lessard, 2000; 9) Mullin et al., 1966.

[a] Estimated from Ray et al. (2001), as a sum of mortality and respiration rate; [b] intercept *x* and size-scaling exponent *y* varied from −0.030 to −0.071 and −1.72 to −1.86, respectively.

winds in the region. This hydrodynamic transport is mainly observed at the near-bottom currents in shallow areas, whereas currents in the deeper regions flow in the opposite direction due to the return flow. Mean depth-averaged currents indicated two major counter rotating gyres within the harbour, contributing to the distinctive transportation and mixing pattern of water quality variables (i.e., suspended solids) in near-shore zone.

Similar to Gudimov et al. (2011), the model was forced by the average hydrological and nutrient loading conditions over the 1996–2010 period in order to reproduce the present water quality conditions prevailing in the Hamilton Harbour. We explicitly considered point and non-point nutrient loads from different sources adjacent to the four spatial segments. The effluents from two of the wastewater treatment plants (Dundas and Waterdown) were added to Cootes Paradise and Grindstone Creek nutrient loading and set to merge into the Cootes Paradise outlet zone. Nutrient loading reduction scenarios were implemented at each source based on the Hamilton Harbour RAP recommendations (see Appendix in Ramin et al., 2011). In particular, the current TP discharges from Woodward (195 kgr day^{-1}) and Skyway (20 kgr day^{-1}) wastewater treatment plants, the Cootes Paradise marsh (38 kgr day^{-1}), the Redhill (21 kgr day^{-1}) and Grindstone (14 kgr day^{-1}) creeks were reduced down to 60, 12, 32, 18, and 12 kgr day^{-1} under the reduced nutrient loading scenario, respectively.

2.3. Allometric configuration of the eutrophication model

We introduced an allometric configuration of the original model, postulating that the various biological rates and interactions among planktonic organisms are partly controlled by their morphological characteristics (Cyr and Pace, 1993; Peters, 1983). Allometric equations were selected mainly based on the availability of regression models in the literature, the domain for which they were developed, as well as the consistency of the outputs for the corresponding parameters (e.g., maximum growth rates, setting velocity rates, nutrient kinetics and quotas) with the calibrated values of the original Hamilton Harbour model (Gudimov et al., 2011). We employed the allometric equation for the maximum growth rate, μ_{max} (day^{-1}) $= 10^{0.54} \cdot V^{-0.15}$ with V in μm^3, obtained from Tang (1995), who used comparable datasets from the literature limited to cultured phytoplankton at saturating irradiance and temperature-normalized growth rate at 20 °C. Although Tang (1995) pointed out that there was no significant effect of the taxonomic affiliation on the estimated maximum growth rates, we used a different equation for the PFG A growth, $\mu_{max} = 10^{0.73} \cdot V^{-0.17}$, to maintain closer to its originally designated attribute of an r-selected organism with higher maximum growth rates; particularly for the small size algal cells. The size dependence of the chlorophyll *a* specific absorption coefficient at 675 nm, within the irradiance range of 25–750 μmol m^{-2} s^{-1}, was based on Fujiki and Taguchi's (2002) empirical equations; $k_{extchla}$ (m^2 mg chl a^{-1}) $= 10^{-x} \cdot V^{-y}$ with values of the intercept x and size-scaling exponent y varying from −0.030 to −0.071 and −1.72 to −1.86, respectively.

We used the Edwards et al.'s (2012) allometric equations to characterize freshwater phytoplankton strategies for nutrient uptake; namely, the half saturation constants for nitrate, NH (μmol N L^{-1}) $= 10^{-0.71} \cdot V^{0.52}$, and phosphorus, KH_P (μmol P L^{-1}) $= 10^{-1.50} \cdot V^{0.53}$, as well as the phosphorus maximum uptake rate, $VP_{maxuptake}$ (μmol P $cell^{-1}$ day^{-1}) $= 10^{-8.40} \cdot V^{0.81}$. We also adopted the allometric relationships between cell volume and intracellular maximum, QP_{max} (fmol $cell^{-1}$) $= 10^{-0.29} \cdot V^{0.767}$, and minimum phosphorus quota, QP_{min} (fmol $cell^{-1}$) $= 10^{-1.04} \cdot V^{0.714}$, as presented by Grover (1989) to examine the influence of cell size and shape on algal competitive ability. Importantly, the expression used to characterize the "cell size", such as cell volume, mass in carbon content, or equivalent spherical diameter, can significantly alter the allometric estimates of physiological and metabolic activity. Tang (1995) suggested that the size effect on maximum growth rate is smaller if algal size is expressed as cell volume than carbon content. To the best of our knowledge, there is no study available to systematically compare the variations of (presumably) equivalent allometric variables in estimating algal physiological rates. Acknowledging the latter source of uncertainty, we considered cell carbon contents obtained from Menden-Deuer and Lessard (2000), and Mullin et al. (1966), only for the purpose of linking the units of allometric estimates of nutrient kinetics ($VP_{maxuptake}$, QP_{max}, and QP_{min}; expressed per cell) to the units of the eutrophication model (expressed per carbon). Algal cell surface area has been also recognized as a regulatory factor for the nutrient kinetics of active transport (Aksnes and Egge, 1991; Litchman et al., 2007; Smith and Kalff, 1982); namely, algal uptake rate is proportional to the number of nutrient ion uptake sites and the handling time at the cell membrane (Aksnes and Egge, 1991; Raven, 1980). Cell surface area relative to their internal storage volume (surface area-to-volume ratio) is often used as a surrogate of the algal capacity to optimize nutrient uptake rates (Aksnes and Egge, 1991; Raven, 1980). For example, algal cells often reduce their cell volume when experiencing nutrient and/or light limiting environments (Marchetti and Cassar, 2009), whereby the number of nutrient transport sites and uptake rates relative to their intracellular nutrient requirement is maximized and/or the diffusion effects at the boundary layer are decreased (Edwards et al., 2012; Hudson and Morel, 1990; Pahlow et al., 1997). Thus, in a post-hoc modeling experiment, we introduced an equation that bases the estimation of phosphorus maximum uptake rate on cell surface area to volume ratio (SA:V) (Friebele et al., 1978).

The empirical relationship used to associate the settling velocity, u_z (m day^{-1}) $= 0.029\ C^{0.42}$, with the carbon cell content (pg C) among marine phytoplankton from Moloney and Field (1991). Many recent size-based models use the same allometric equation for algal settling (Gin et al., 1998; Nogueira et al., 2006; Sin and Wetzel, 2002). Generally, empirical equations to characterize the dependence of algal sinking rates on cell morphology are somewhat rare in the literature partly due to the difficulty in estimating the settling rates of living organisms, which depend not only on the particle size but also on buoyancy mechanisms of certain species, the cell shape, and the physical characteristics of the water column (Anderson et al., 1985; Hurtt and Armstrong, 1996). Along the same line of reasoning, the size dependent losses due to respiration and mortality were provided by Ray et al.'s (2001) empirical equation m_p (day^{-1}) $= 10^{-0.063} \cdot V^{0.008}$. Because no empirical equation was available in the literature to directly characterize the size dependence of the zooplankton nominal preference for phytoplankton (*Pref*), we assigned coefficients such that the maximum and minimum cell volumes considered (when expressed in logarithmic scale) produce values between 0.5 and 1.5 (Gudimov et al., 2010). For illustration purposes, the allometric configuration of the current model was solely focused on the phytoplankton governing equation, although on-going research revisits the zooplankton functional group characterization in a similar manner.

2.4. Monte Carlo analysis

Our analysis examines the role of cell morphology of the phytoplankton groups typically observed in the Hamilton Harbour, and their competitive capacity under the present and the reduced phosphorus loading scenarios. To accommodate the size variability within the same functional groups, we assigned a range of cell volumes to each functional group (PFG A, PFG B and PFG C), between 0.1 μm^3 and 2000 μm^3 to run Monte Carlo simulations (Fig. 1 in Electronic Supplementary Material or Fig. S1). While we recognize that species of dinoflagellates (>40,000 μm^3) or cryptomonads (3–6000 μm^3) have considerably larger volumes, we note that many of the available allometric equations were developed within the size range used in our analysis, and therefore provide unrealistic estimates when applied to extrapolate biological rates. The parametric uncertainty of the allometric regressions was also considered by propagating the corresponding

standard error estimates through our simulations. When the error estimate was not reported in the original study (see references in Table 1), we recreated the corresponding allometric relationship by digitizing the corresponding graphs. The characterization of the rest features of phytoplankton functional groups remained intact from our earlier modeling work (Gudimov et al., 2010, 2011; Ramin et al., 2011, 2012). The optimal temperatures for the growth rates of the three functional groups were set equal to 20 °C, 22 °C, and 24 °C, respectively (Table 2). Thus, PFG C bears resemblance to cyanobacteria in regard to its higher temperature optima (Johnk et al., 2008; Shimoda et al., 2011). In addition, the same functional group is characterized by lower half saturation constants for light intensity and ammonium uptake as well as lower assimilation efficiency for zooplankton. Similar to the protocol presented by Zhao et al. (2008a,b), we also induced perturbations of the reference abiotic conditions, uniformly sampled from the range ±25%, to accommodate the interannual variability in nutrient loading, exchange with Lake Ontario, solar radiation, epilimnetic/hypolimnetic temperature, and vertical diffusion. In a similar manner, we incorporated daily noise representing the intra-annual abiotic variability (Arhonditsis and Brett, 2005). For each of the two loading scenarios, we generated 4000 input vectors independently sampled from 35 (3 × 10 model parameters/functional properties and 5 forcing functions) probability distributions, which then were used to run the model for 10 years. Finally, we generated two (4000 × 12 × 8) output matrices that comprised the average monthly epilimnetic values for the three phytoplankton functional group and total zooplankton biomass, dissolved inorganic nitrogen (DIN), total nitrogen (TN), phosphate (PO_4), and total phosphorus (TP) concentrations.

3. Results–discussion

3.1. Model calibration–characterization of the phytoplankton functional group dynamics

For the purpose of model calibration, the default cell volume values assigned to the phytoplankton functional groups A (2000 μm^3), B (800 μm^3), and C (200 μm^3) aimed to characterize the typical diatom (*Stephanodiscus niagarae, Fragilaria crotonensis*), chlorophyte/cryptophyte (*Coelastrum asteroideum, Coelastrum reticulatum, Scenedesmus braziliensis, Oocystis lacustris, Cryptomonas reflexa, Rhodomonas minuta*), and cyanobacteria (*Aphanizomenon flos-aquae, Lyngbya birgei, Anabaena crassa, Chroococcus limneticus, Microcystis aeruginosa, Woronichinia naegeliana*) assemblages in the Hamilton Harbour. The calibration exercise was mainly intended to serve as an exploratory analysis of the model as well as an opportunity to gain insights into the simulated interspecific competition patterns during the summer stratified period. Except from the allometric properties, the rest model parameters remained practically unaltered in order to maintain the ecosystem characterization from our earlier modeling work (Table 2; see also Table S2). Similar to the Gudimov et al.'s (2011, 2010) strategy, our calibration was focused on the model ability to realistically reproduce the average water quality conditions and to characterize the epilimnetic planktonic processes (Dermott, 2007; Hiriart-Baer et al., 2009). The comparison between model outputs in the four spatial segments and observed monthly averages from 1996 to 2010 is also combined with the 95% uncertainty bounds that depict the observed variability (Figs. S2–S3; see also following discussion). Generally, the model accurately reproduces the average phosphate, total phosphorus, nitrate, total ammonia, total nitrogen, chlorophyll *a*, and total zooplankton biomass patterns, and also predicts consistently higher nutrient levels in the spatial segment influenced by the Woodward wastewater treatment plant.

The model accurately predicts the winter maxima (≈12.0 μg L^{-1}) and the summer minima (≈2.5–4.0 μg L^{-1}) of the epilimnetic phosphate levels. Likewise, the model closely reproduces the summer epilimnetic TP levels (35–40 μg L^{-1}) as well as the observed total ammonia variability in the system. We also found significant agreement between predicted and observed winter and spring nitrate concentrations, although the model seems to underestimate the summer epilimnetic and hypolimnetic (not presented here) levels. Aside from the assigned nitrification rates in the water column and/or the sediments, one plausible explanation may be the substantial uncertainty associated with the external loading estimates, as we are lacking reliable information on the nitrate/nitrite concentrations in all the major point and non-point sources; especially after the upgrades to the nitrification facilities in the local wastewater treatment plants. Nitrate/nitrite concentrations have been increasing at an accelerating rate for almost four decades in the harbour (Barica, 1989). While concentrations are well below the Canadian Water Quality Guideline of 13 mg L^{-1}, their implications for the ecosystem functioning remain to be assessed (Hiriart-Baer et al., 2009). According to the model predictions, the TN concentrations can reach the level of 3–4 mg L^{-1} during the winter and may drop down to 1.5 mg L^{-1} during the summer stratified period. The model closely reproduces the winter (≈5 μg chlα L^{-1}) and the summer (≈15–20 μg chlα L^{-1}) phytoplankton levels, but overpredicts the spring chlα concentrations as a major spring phytoplankton bloom exceeding 20 μg chlα L^{-1}. According to the model predictions, the average epilimnetic primary productivity rate at optimal irradiance levels is approximately 45–50 mg C $m^{-3}h^{-1}$ during the summer season, which falls within the 36–75 mg C $m^{-3}h^{-1}$ range reported by Munawar and Fitzpatrick (2007). Our model also predicts two major peaks of the total zooplankton biomass; the first peak follows the spring phytoplankton bloom (≈200 μg C L^{-1}) while the second one is predicted to occur at the end of summer-early fall (≈180 μg C L^{-1}). These predictions match closely the observed patterns reported by Munawar and Fitzpatrick (2007), e.g., Figs. 8–9; pages 62–63, if we assume an average wet to dry biomass of 10, along with 0.4 μg C per μg of dry zooplankton biomass (Downing and Rigler, 1984). Similar to the observed patterns,

Table 2
Differences in the physiological characteristics of the three phytoplankton functional groups (PFGs) based on model calibration.

Calibrated parameters	Symbol	PFG A	PFG B	PFG C	Unit	Sources
Fraction of algal mortality becoming dissolved organic carbon	α_{DOC}	0.5	0.5	0.5	–	1
Fraction of algal mortality becoming ammonium	α_{NH4}	0.5	0.5	0.5	–	1
Fraction of algal mortality becoming phosphate	α_{PO4}	0.25	0.25	0.25	–	Calibration
Herbivorous zooplankton assimilation efficiency for phytoplankton	$asfood_{herbi}$	0.5	0.5	0.15	–	2
Omnivorous zooplankton assimilation efficiency for phytoplankton	$asfood_{omn}$	0.5	0.5	0.15	–	2
Chlorophyll to carbon ratio in phytoplankton	*ChlaC*	0.02	0.02	0.02	–	3–6
Half saturation light intensity for phytoplankton	*Ik*	150	150	125	MJ m^{-2} day^{-1}	11, Calibration
Effect of temperature on phytoplankton	*KTgr*	0.004	0.004	0.004	$°C^{-2}$	1,7–9
Water reference temperature	$Temp_{ref}$	20			°C	1,5,7,10
Half saturation constant for algal ammonium uptake	*AH*	100	80	60	mg N m^{-3}	6,8,9
Strength of the ammonium inhibition for nitrate uptake	ψ	0.05	0.05	0.045	$(\mu g\ N/L)^{-1}$	Calibration
Optimal temperature for algal growth	*Topt*	20	22	24	°C	1,5,7,10

1) Cerco and Cole, 1993 (and references therein); 2) Gudimov et al., 2011; 3) Wetzel, 2001; 4) Chen et al., 2002 (and references therein); 5) Reynolds, 1984; 6) Hamilton and Schladow, 1997 (and references therein); 7) Omlin et al., 2001; 8) Arhonditsis and Brett, 2005; 9) Reynolds, 2006; 10) Jorgensen et al., 1991.

the simulated proportion of omnivorous to herbivorous zooplankton varies between 25 and 50% during the seasonal cycle.

We then examined the role of algal cell size, the allometrically-derived maximum phosphorus uptake rates as well as the zooplankton grazing control on the relative abundance of the algal assemblages modeled. For illustration purposes, we present the inference drawn from the simulated patterns of the functional groups A and C during the mid-summer stratified period, when frequent cyanobacteria blooms occur in the system (Figs. 2 and 3). In general, within the cell volume range examined, small species have a distinct competitive advantage across the nutrient loading conditions reproduced (Figs. 2a, b and 3a, b). This pattern was more pronounced with the functional group C, which achieves faster growth rates due to the higher temperature optimum assigned. The sigmoid model fitted to the phytoplankton abundance medians of each cell size bin suggests that the highest median value of 11 μg chla L^{-1} is realized with cell sizes lower than 400 μm^3 under the present ambient nutrient levels, while algal cells larger than 1000 μm^3 asymptotically tended to a median abundance level of 2 μg chla L^{-1}. The sharpest PFG C biomass increase occurred within the cell volume range of 400 to 1000 μm^3, where the fitted sigmoid model suggests an increase of the odds to exceed the level of 11 μg chla L^{-1} by 2.58 (or $e^{0.95}$) each time the cell size increases by 100 μm^3. Importantly, the corresponding minimum and maximum estimates of the median abundance levels decreased down to 1 and 5 μg chla L^{-1},

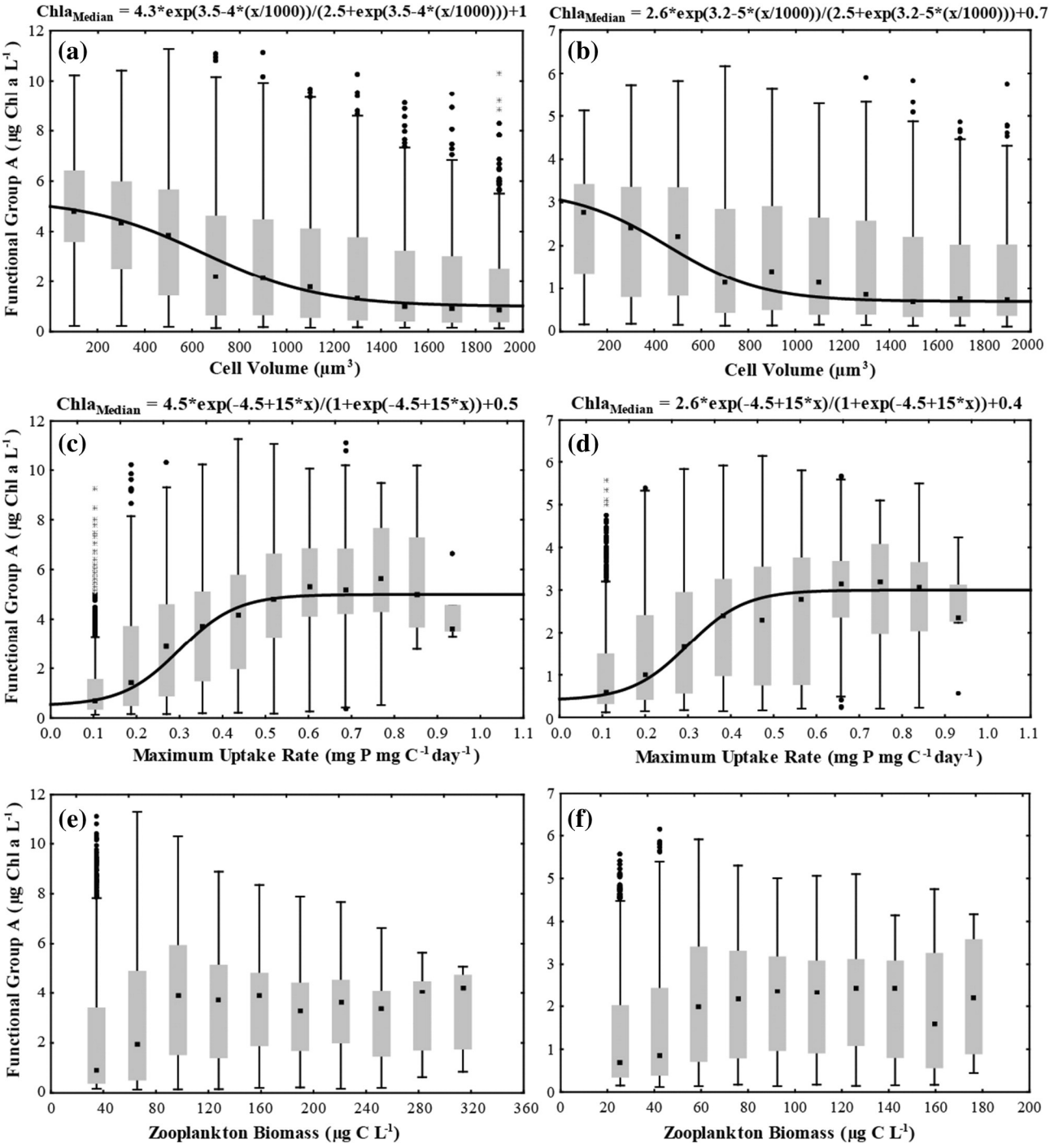

Fig. 2. Response of the phytoplankton functional group A during the end-of-summer stratified period, as a function of the (a, b) cell volume; (c, d) maximum uptake rate, and (e, f) zooplankton biomass under present (left panels) and reduced nutrient loading conditions (right panels).

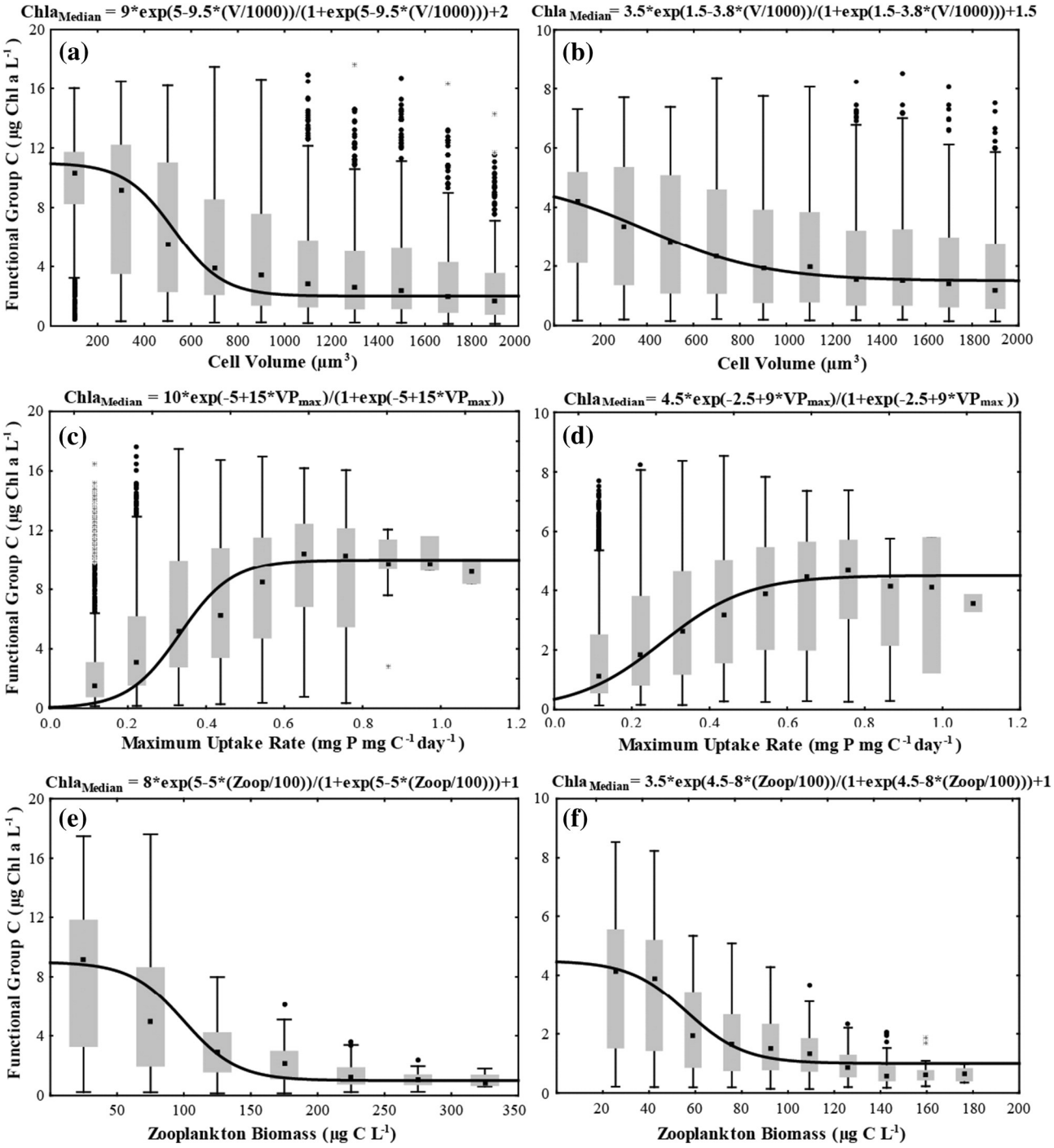

Fig. 3. Response of the phytoplankton functional group C during the end-of-summer stratified period, as a function of the (a, b) cell volume; (c, d) maximum uptake rate, and (e, f) zooplankton biomass under present (left panels) and reduced nutrient loading conditions (right panels).

when the model was forced with the reduced nutrient loading scenario. On the other hand, the lower growth rates moderated the response of the functional group A to cell size variability at warm water temperatures, with an approximate 1.49 (or $e^{0.40}$) increase of the odds to exceed the 5.3 µg chla L^{-1} level for each 100 µm^3 incremental increase of the PFG A cell size within the 400–1000 µm^3 range. There was also a notable decrease of the maximum median abundance level (2.7 µg chla L^{-1}) for that assemblage with the reduced nutrient loading scenario.

Among the allometric parameters considered, the changes of the maximum phosphorus uptake rate induced by the algal cell size were particularly pronounced, indicating a significant algal biomass increase within the range of 0.20–0.45 µg P µg C^{-1} day^{-1} which levels off thereafter (Figs. 2c, d and 3c, d). For a given functional group and nutrient loading regime, this pattern is translated into an approximate 4.48 (or $e^{1.50}$) increase of the odds to exceed the corresponding maximum estimate of the median biomass level each time the phosphorus uptake rate increases by 0.01 µg P µg C^{-1} day^{-1}. In our analysis, we used a two-pronged allometric approach to estimate the amount of phosphorus per time that is transported into the algal cells as a function of their morphology, which is subsequently scaled over the cellular carbon content (Edwards et al., 2012; Menden-Deuer and Lessard, 2000). The propagation of the standard error of the two empirical equations entails considerable uncertainty with increasing algal cell volumes or surface-to-volume ratios, and therefore further refinement of these

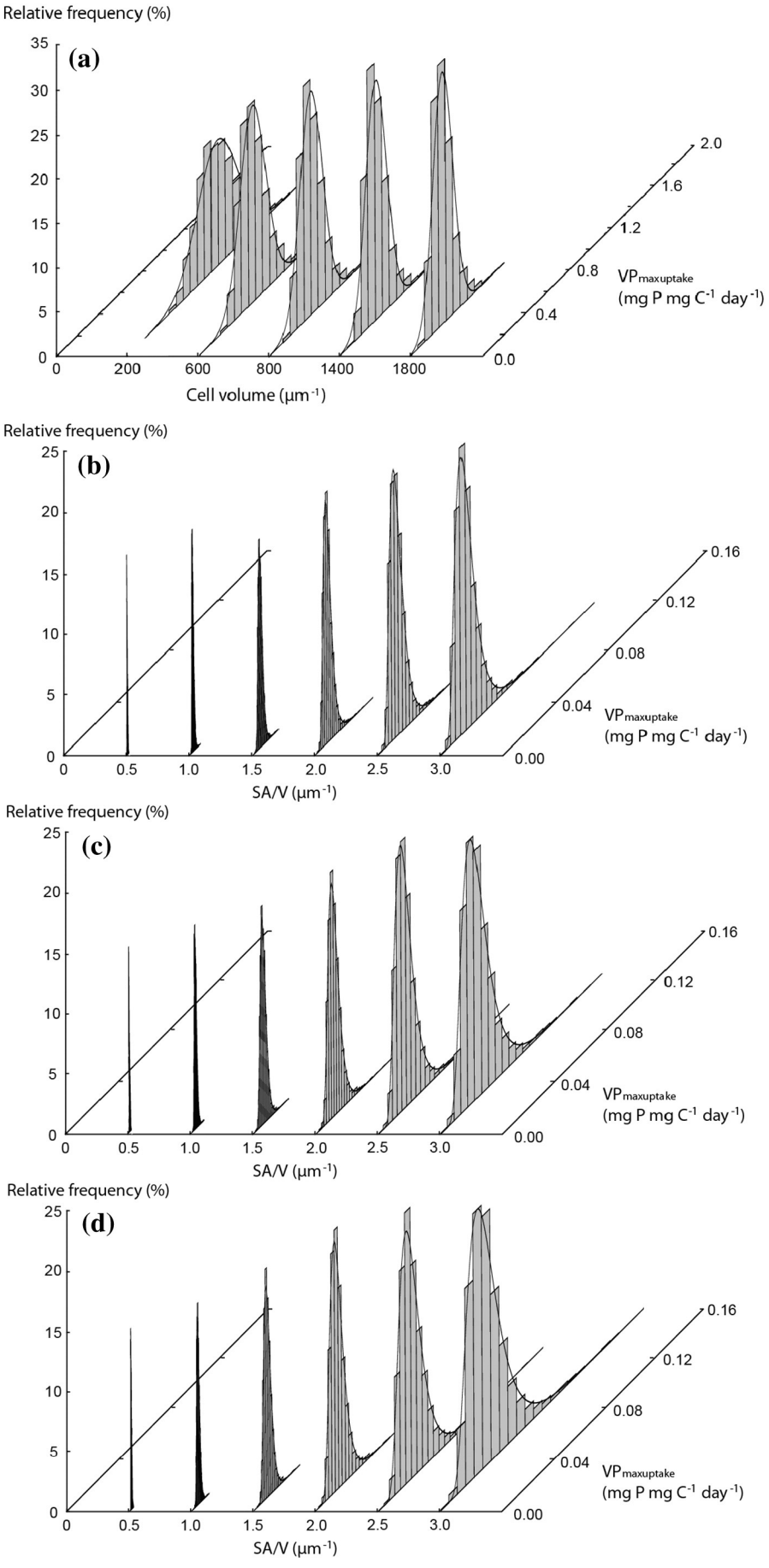
Relative frequency (%)
(a)
Cell volume (μm-1)
VPmaxuptake
(mg P mg C-1 day-1)
Relative frequency (%)
(b)
SA/V (μm-1)
VPmaxuptake
(mg P mg C-1 day-1)
Relative frequency (%)
(c)
SA/V (μm-1)
VPmaxuptake
(mg P mg C-1 day-1)
Relative frequency (%)
(d)
SA/V (μm-1)
VPmaxuptake
(mg P mg C-1 day-1)

allometric relationships would improve the credibility of our phytoplankton simulations (Fig. 4; see also following discussion). Our model also postulates that the competitive advantage rendered by the superior nutrient uptake kinetics of smaller algal cells could be counterbalanced by the higher zooplankton grazing pressure. In this context, we note that the control exerted by the herbivores is particularly evident with the functional group C, and less so with the abundance of the algal assemblage A (Figs. 2e, f and 3e, f). Alongside with the prespecified nominal preferences and assimilation rates, our model assumes that zooplankton preferentially feeds upon the most abundant prey items, and therefore the functional group C becomes the primary staple of the zooplankton diet during the summer period when its annual biomass maxima occur. Notably, our Monte Carlo analysis suggests a 1.64 (or $e^{0.50}$) decrease of the odds to exceed the maximum median PFG C abundance value (9.0 μg chla L^{-1}) for each 10 μg C L^{-1} incremental zooplankton biomass increase within the 50–150 μg C L^{-1} range.

The abundance of total phytoplankton and the three functional groups over the entire range of end-of-summer TP levels generated by the present and reduced nutrient loading regimes are provided in Fig. 5. Our model predicted a non-linear (sigmoid) total phytoplankton biomass vs TP relationship, which suggests that the highest median phytoplankton biomass values (>14 μg chla L^{-1}) are realized when the ambient phosphorus levels exceed the level of 34 μg TP L^{-1}, while the reduced nutrient loading conditions will result in a median phytoplankton abundance lower than 8 μg chla L^{-1} (Fig. 5a). Bearing in mind the constraints imposed by the discontinuity of our Monte Carlo samples (i.e., two nutrient loading regimes examined), we note that the sharpest algal biomass decline occurred within the TP range of 16 to 30 μg TP L^{-1} in which the fitted sigmoid model suggests a decrease of the odds to exceed the predicted maximum median level of 14 μg chla L^{-1} by 1.65 (or $e^{0.50}$) each time the end-of-summer TP is reduced by 2 μg L^{-1}. Interestingly, our model predictions suggest that the total chl*a* values at the lower end of the present nutrient loading scenario (20–24 μg TP L^{-1}) deviate from the general monotonic pattern, and this trend is associated with the disproportional biomass increase of the algal assemblage C (Fig. 5d). Likewise, the median biomass of the same functional group demonstrates a counterintuitive negative relationship with the ambient TP levels contrary to the positive trends characterizing the assemblages A and B (Fig. 5b, c). A careful inspection of the cell volume distributions associated with the corresponding TP concentration bins suggests that this pattern mainly arises when the functional group C is assigned smaller cell volumes, i.e., <600 μm^3 (Fig. 6c), and becomes even more pronounced when the other two functional groups are specified as large species (Fig. 6c). Coupled with the other attributes prescribed to this group (low half saturation constant for ammonium and light intensity, higher temperature optimum to experience maximum growth rates), these numerical experiments not only rendered an overwhelming competitive advantage to PFG C but also made the chlorophyll a versus total phosphorus relationship distinctly steeper, i.e., higher algal biomass is sustained within a given ambient TP level.

3.2. Modeling summer algal blooms

Hamilton Harbour experiences erratic outbreaks of noxious and toxin-producing cyanobacteria (*Microcystis*), despite the substantial decrease of the TP levels in the system (Murphy et al., 2003). These patterns of cyanobacteria dominance may seem counterintuitive as the existing paradigm suggests that their capacity to outcompete the usual eukaryotic residents of the summer phytoplankton communities decreases under low phosphorus availability (Hyenstrand et al., 2001; Watson et al., 2008). Although several hypotheses have been examined to explain this abrupt structural shift in the summer algal assemblage, recent empirical evidence suggests that one potential culprit could be the hypolimnetic phosphate accumulation, which can reach excessively high levels (>60 μg P L^{-1}) during the late summer/early fall period, depending on the thickness of hypolimnion and hydraulic exchange rates with Lake Ontario (Gudimov et al., 2011). This pattern underscores the likelihood of the summer epilimnetic environment to be subjected to intermittent nutrient pulses from the hypolimnion, which in turn may have important implications for the abundance, composition or even predictability of the phytoplankton community (Jorgensen and Padisak, 1996; Soranno et al., 1997). Despite all the arguments historically used to downplay the relative contribution of the sediment fluxes in the system (Mayer and Manning, 1990), Loh et al. (2013), presented empirical evidence of summer episodes of internal P loading can be conceivably linked to the protracted hypolimnetic hypoxia of the system (Gudimov et al., 2010). Thus, given also that the hypoxia in the harbour waters will continue to be an issue (Charlton, 2001), the likelihood of the internal loading to trigger undesirable shifts on the epilimnetic summer assemblage and/or to exert control on the water quality conditions warrants further investigation.

To emulate the hypolimnetic phosphorus accumulation during the summer period, we induced a tenfold increase of the PO_4 concentrations during the mid-summer period, which may then influence the epilimnetic phytoplankton patterns through advective and diffusive vertical transport. This scenario aimed to reproduce the prevailing conditions in the Hamilton Harbour during the summer of 2012. Our exercise was also intended to examine the capacity of the allometric phytoplankton characterization to reproduce the end-of-summer algal blooms. In this regard, we introduced a new equation that connects the maximum phosphorus uptake rate with the cell surface-to-volume ratio (SA/V) instead of the cell volume (Friebele et al., 1978; see Table 1). The latter modification aimed to accommodate the idea that small-sized species with higher SA/V values may achieve more rapid nutrient transfer and potentially dominate environments that experience fluctuations in resource supply (Grover, 1991; Stolte and Riegman, 1996). On the other hand, large cell species have been hypothesized to possess greater nutrient storage ability, and thus to increase in abundance with increasing nutrients, such as intermediate frequency nitrogen pulses (Cavender-Bares et al., 2001; Li, 2002; Litchman et al., 2009). Alongside with the new maximum phosphorus uptake rate expression, we examined the sensitivity of the functional group dynamics to the optimal temperature for growth. First, given the original cell volume values assigned to the phytoplankton functional groups A, B, and C along with a universally constant SA/V (=2.5 μm^{-1}), the corresponding optimum temperatures were set equal to 18, 21, 24 °C (Fig. 7a–d) and 20, 21, 22 °C (Fig. 7e–h). The objective of the former specification was to magnify the physiological difference among the functional groups A and C, thereby rendering them competitive advantage during the spring and summer periods, respectively. With the second scenario, the SA/V values for PFG A, PFG B, and PFG C were correspondingly set equal to 3, 2.5, 2 μm^{-1} (Fig. 8a–d), and 2, 2.5, 3 μm^{-1} (Fig. 8e–h).

The model consistently reproduced a distinct secondary algal peak toward the end-of-summer period, predominantly triggered by the hypolimnetic PO_4 accumulation, although the dynamics of the three functional groups differed among the scenarios examined. The modeling experiment with the different temperature specifications indicated that the three competitors almost equally capitalized upon the nutrient

Fig. 4. Maximum phosphorous uptake rate ($VP_{maxuptake}$) derived from two equations; (a) $VP_{maxuptake} = 10^{-8.4}\, V^{0.81}$ (Edwards et al., 2012) and normalized with $C = 10^{-0.665}\, V^{0.939}$ (Menden-Deuer and Lessard, 2000), and (b–d) $VP_{maxuptake} = 10^{-10.7} SA/V^{1.7}$ (Friebele et al., 1978), normalized with $C = 10^{-0.29}\, V^{0.76}$ (Mullin et al., 1966). The distributions depicted for each cell volume and SA/V ratio represent the parametric uncertainty of the allometric equations. Maximum phosphorus uptake rates plotted in panels (b), (c), and (d) were based on cell volumes 200, 800, and 2000 μm^3, respectively.

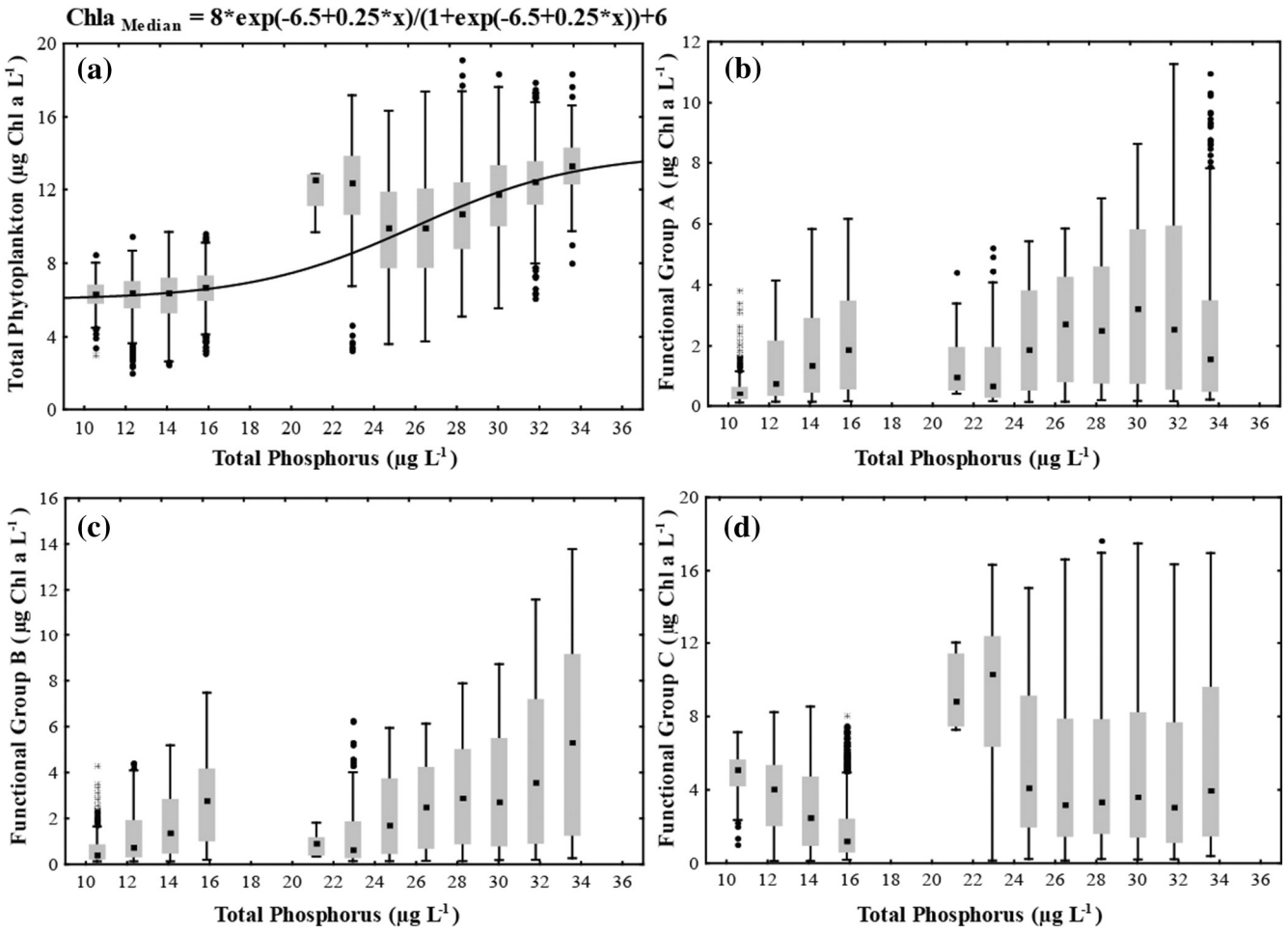

Fig. 5. Phytoplankton biomass against the end-of-summer total phosphorus concentrations; (a) total phytoplankton, and (b–d) phytoplankton functional groups A, B and C.

intrusions from the hypolimnion, and therefore their relative contribution to the total algal biomass remained practically unaltered (Fig. 7). On the other hand, the surface-to-volume ratio is a critical feature that significantly invigorates the adaptive specialism of competing species (Fig. 8). It is also important to note that the hypolimnetic nutrient pulses were able to stimulate significant algal blooms (>8–10 chla µg L^{-1}) even under the reduced exogenous nutrient loading conditions. In particular, algal species with high SA/V values gained competitive advantage after events of enhanced entrainment of nutrient-rich hypolimnetic waters, albeit their low relative abundance during the rest of the annul cycle (Fig. 8f–h). The latter prediction casts doubt on the likelihood to eliminate the occurrence of harmful algal blooms and consolidate the future resilience of the system, unless the potential mechanisms responsible for the hypolimnetic accumulation (e.g., sediment diagenesis) are more effectively mitigated (Gudimov et al., 2011). When we assigned a narrow T_{opt} range and therefore the temperature control of the growth for the three functional groups was fairly similar (20–22), the algal assemblage C became the predominant group during the spring period. From a technical standpoint, the latter observation reinforces our earlier assertion that the phytoplankton seasonal succession pattern during the model calibration was mainly obtained due to the group-specific temperature preferences (Fig. S2), and otherwise the designated smaller species (PFG C) possesses the most advantageous traits for resource competition. On a final note, although the present model structure disallowed the examination of relevant ecological pathways (see following discussion), the hypolimnetic phosphorus accumulation could also trigger the predominance of species that have the capacity to vertically migrate and exploit favorable environments.

4. Conclusions–future perspectives

Our growing knowledge of the functioning of aquatic systems has highlighted the need to improve the performance of mathematical models by explicitly treating multiple biogeochemical cycles, increasing plankton food web diversity, and refining the mathematical description of higher trophic levels (Anderson, 2005; Arhonditsis and Brett, 2005; Fennel, 2008). However, the increased model complexity entails more degrees of freedom (calibration parameters) that may -in principle- provide good fit to any data set, but also reduce our ability to properly constrain model parameters from observations; namely, these reductionistic modeling strategies inflate the disparity between what ideally we want to tease out from a model and what can realistically be observed in the real world, thereby maximizing the likelihood to achieve "good results for the wrong reasons" (Arhonditsis, 2010; Arhonditsis et al., 2007b). Striving for the development of parsimonious modeling constructs, we introduced the allometric characterization of phytoplankton physiological processes as a universally applicable property that can effectively reduce the number of tunable parameters (Poulin and Franks, 2010). Our work stipulates that the allometric specification of biological rates can partly accommodate the wide range of physiological traits typically manifested within the same taxonomic affiliation (Kruk et al., 2010; Segura et al., 2013). While far from being a flawless depiction of the real world (Flynn, 2005), we argue that this strategy

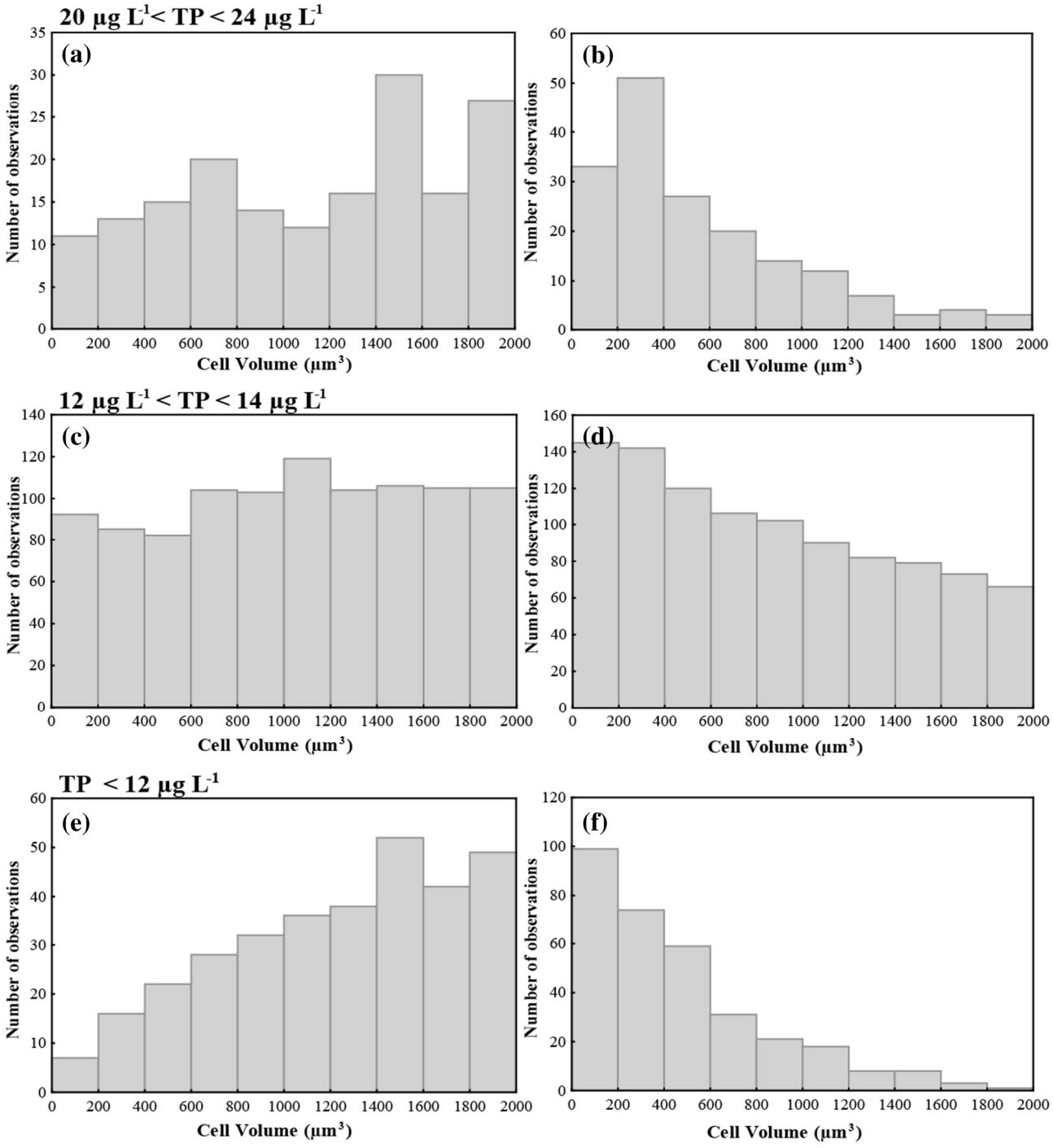

Fig. 6. Distribution of the cell volumes for phytoplankton functional group A (left panels) and C (right panels) for three TP concentration ranges.

has several advantages that should improve the operational capacity of the current generation of process-based models. The major lessons learned from our modeling analysis are as follows:

- The allometric configuration of the eutrophication model reasonably reproduced the observed phosphate, total phosphorus, nitrate, total ammonia, total nitrogen, chlorophyll *a*, and total zooplankton biomass patterns in Hamilton Harbour. Importantly, our analysis showed that the implementation of the nutrient loading reductions proposed by the Hamilton Harbour RAP will improve the water quality conditions in the system, as it can be inferred by the significant decrease of the predicted chlorophyll a and TP values. Consistent with empirical evidence, our modeling analysis showed that small algal species have a distinct competitive advantage in summer epilimnetic environments across the range of cell volume and nutrient loading conditions examined; especially, when they are characterized by higher optimal temperature for growth. Small-sized algal species possess superior nutrient utilization traits due to their high surface area-to-volume ratios and maximum growth rates, thereby gaining competitive advantage in nutrient limiting and enriched environments, respectively (Banse, 1982; Litchman et al., 2009). Counter to the Edwards et al.'s (2012) findings though, it is worth noting that small cells were also assigned lower half saturation constants for phosphate uptake and thus our experiments may have somewhat overstated their dominance. In a similar manner, additional factors that could further modulate the competition patterns are

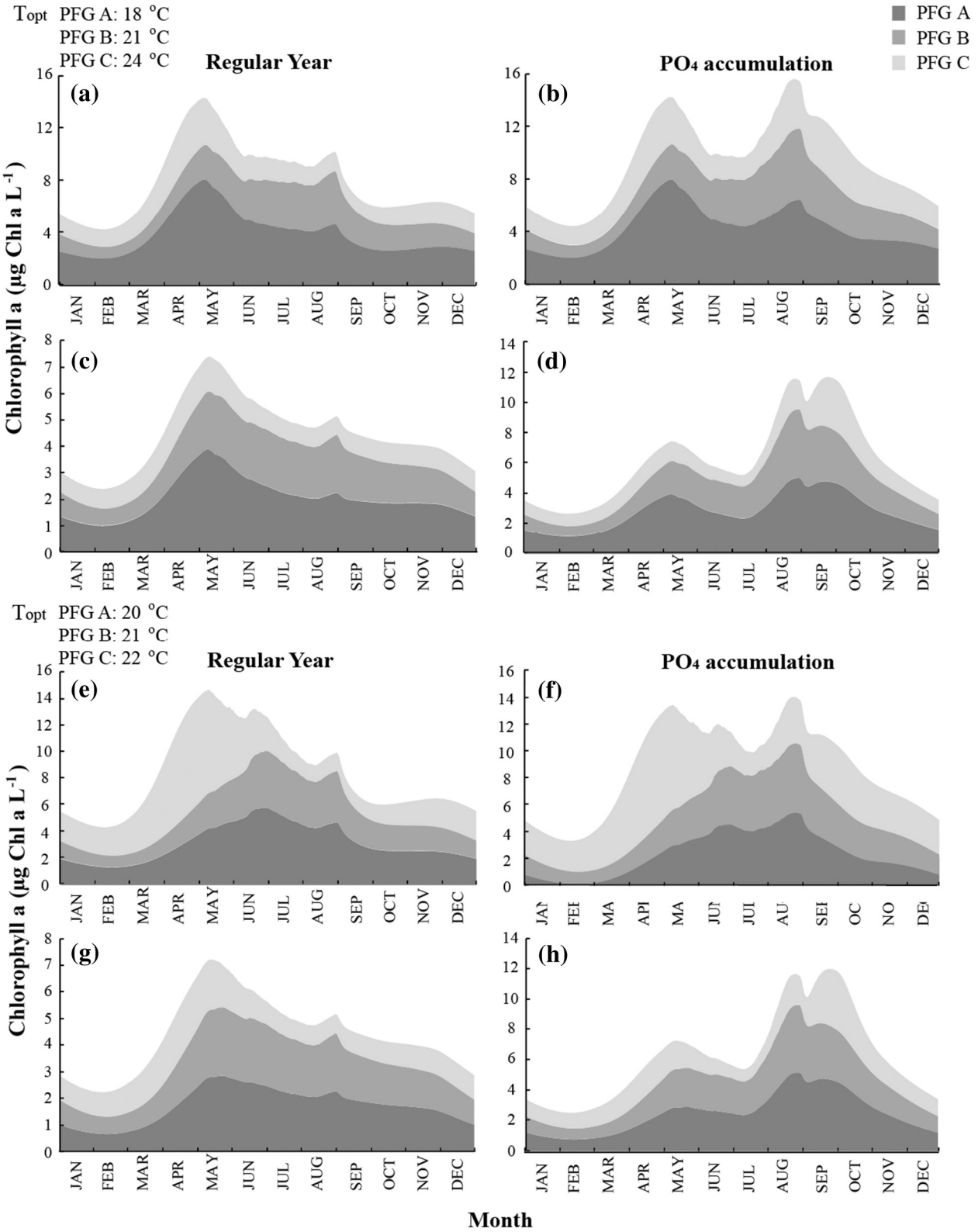

Fig. 7. Phytoplankton competition patterns under present (a, b, e, f) and reduced phosphorus loading conditions (c, d, g, h). Right panels represent an additional scenario of hypolimnetic phosphate accumulation after the mid-summer period. Cell volume: PFG A = 2000 µm^3; PFG B = 800 µm^3; and PFG C = 200 µm^3. Cell surface area-to-volume ratio: 2 µm^{-1} (all PFGs). Optimal temperature for growth: PFG A = 18 °C; PFG B = 21 °C, and PFG C = 24 °C. Panels (e) to (h) are based on optimal temperatures for algal growth equal to 20 °C, 21 °C and 22 °C, respectively.

the shape of algal species, e.g., large elongated cells are often better competitors than small spherical ones (Grover, 1989), and the nutrient supply mode, e.g., intermediate frequency nitrogen pulses can select for large-sized species but constant/pulsed phosphorus supply select for small sizes (Litchman et al., 2009). Further, the mathematical description of nutrient procurement rates of colonial or filamentous forms is another understudied aspect that requires reliable empirical support (Pahlow et al., 1997; Serizawa et al., 2008).

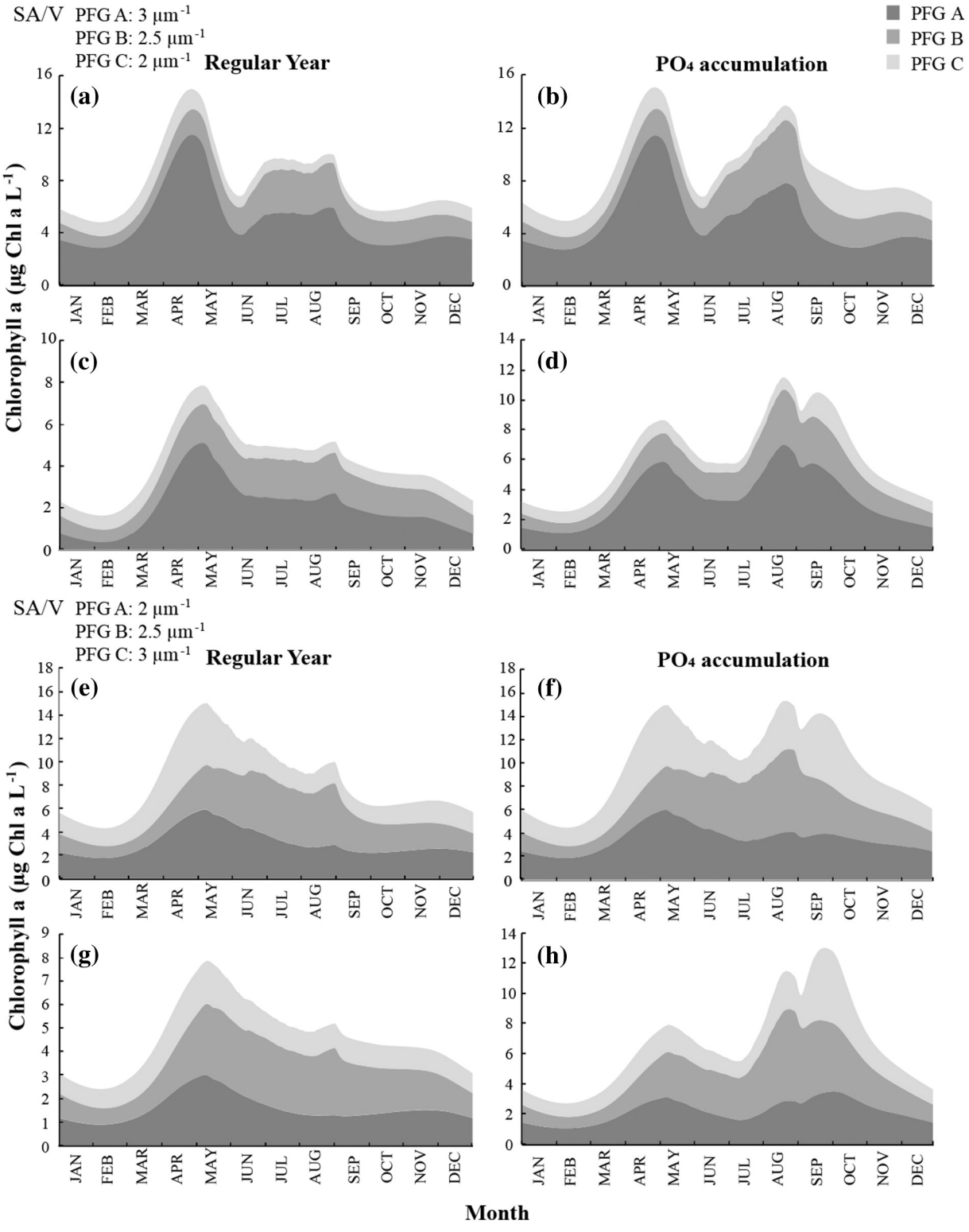

Fig. 8. Phytoplankton competition patterns under present (a, b, e, f) and reduced phosphorus loading conditions (c, d, g, h). Right panels represent an additional scenario of hypolimnetic phosphate accumulation during the end-of-summer stratified period. Cell volume: PFG A = 2000 μm^3; PFG B = 800 μm^3; and PFG C = 200 μm^3. Optimal temperature for algal growth: PFG A = 18 °C; PFG B = 21 °C; and PFG C = 24 °C. Panels (a) to (d) are based on SA/V values equal to 3 μm^{-1}, 2.5 μm^{-1} and 2 μm^{-1} for PFG A, B and C, respectively. Panels (e) to (h) are based on SA/V values equal to 2 μm^{-1}, 2.5 μm^{-1} and 3 μm^{-1} for PFG A, B and C, respectively.

· Strong top-down pressure mediated by high zooplankton abundance effectively controls the standing biomass of phytoplankton species that can otherwise realize high growth rates under the conditions typically prevailing in the end-of-summer epilimnetic environments (e.g., higher temperature optima, higher tolerance in low water clarity). This finding is conceptually on par with empirical evidence that intense herbivory rates act as a "safety valve", suppressing phytoplankton groups with size-based strategies for resource procurement under the ambient phosphorus levels and prohibit major structural shifts in algal assemblages (Cottingham and Schindler, 2000; Cottingham et al., 2004). By contrast, when the summer community is released by the zooplankton grazing,

the exceedance of critical phytoplankton biomass levels and the likelihood of harmful algal blooms are determined by the multitude of factors that shape inter-specific competition patterns (e.g., relative abundance of competing species, nutrient uptake kinetics). One of the future challenges associated with the allometric approach to plankton modeling involves the characterization of dependence of prey-predator relationships on size structure (Hansen et al., 1994; Wirtz, 2013, 2014). In our model, the strength of trophic interactions between primary producers and grazers was approximated by the causal linkage between grazing preference and size of prey items, although the narrow biovolume range examined disallowed the full assessment of its importance. In addition, empirical efforts to depict the zooplankton somatic growth submodel as a function of the interplay among prey morphology, nitrogen, phosphorus, highly unsaturated fatty acids, and other potentially important metabolic congeners through the grazers' digestive tracks are profoundly missing (Perhar et al., 2012).

- Regarding the mechanisms that drive non-linear shifts in the phytoplankton community of the Hamilton Harbour, our modeling analysis showed that the high hypolimnetic phosphate concentrations can induce profound changes in the algal abundance and composition during the late summer/early fall period. Importantly, algal species with high cell surface-to-volume ratios can easily dominate the summer assemblage after intrusion events of nutrient-rich hypolimnetic waters. Viewed from this perspective, the role of sediments as a potential source of nutrients could be a central theme for the future system management and may be further magnified by the projected shift to a warmer climate. For example, a combination of longer and stronger thermal stratification along with reduced hydrodynamic exchanges with Lake Ontario (i.e., lower inflow rates of low nutrient and well oxygenated waters) could exacerbate the hypoxia conditions and the internal loading in the system, which in turn may negate any improvements that are likely to be brought about by the reduced exogenous nutrient loading conditions (Gudimov et al., 2010; Ramin et al., 2012). In the same context, recent empirical evidence suggests that prolonged summer episodes of internal loading are accompanied by Fe fluxes that can be conceivably linked to the phosphorus–ferrous model (Loh et al., 2013; Molot et al., 2014). This model states that while phytoplankton productivity is controlled by P, significant diffusion of Fe^{+2} from anoxic sediments into waters near the euphotic zone is a prerequisite for cyanobacteria bloom formation (Molot et al., 2010). Because of their higher cellular iron requirements, cyanobacteria dominance could be triggered when ferrous iron levels are elevated in the system. There are two compelling reasons why this hypothesis warrants further investigation: (i) even if the RAP nutrient loading reduction measures come into effect, the duration and severity of hypoxia in the Hamilton Harbour will likely not improve significantly (Charlton, 2001), and thus the occurrence of internal loading events cannot be ruled out; and (ii) the phosphorus–ferrous model offers a reasonable explanation for the cyanobacteria outbreaks in mesotrophic (intermediate productivity) systems with TP concentrations below 20 μg L^{-1} that supposedly have low risk of bloom formation (Molot et al., 2014)
- An appealing prospect of the allometric approach is the capacity to effectively link sampling efforts and/or experimentation with the structure optimization or the reduction of uncertainty of our modeling constructs. Model calibration is not merely viewed as an inverse solution exercise, whereby the data collection involves only the model outputs and subsequently the parameters are adjusted to obtain good fit between observations and predictions. We rather argue that the model parameter estimation requires guided experimentation that revolves around the development/refinement of the allometric characterization of model parameters. In this study, we found that several of the empirical equations used were based on small sample size (low degrees of freedoms), were not available for the particular type of ecosystems modeled, and/or only captured a fairly narrow range of cell sizes typical encountered in natural ecosystems. Another example is the use of two empirical models that connect the maximum phosphorus uptake rate with the cell volume and the surface-to-volume ratio, which provided estimates of the nutrient transport kinetics with considerable difference (Fig. 4). This discrepancy reflects the nature of the dataset used for these empirical models, e.g., eleven phytoplankton species from Rhode River used in Friebele et al. (1978) vis-à-vis the assemblage of 124 freshwater species compiled by Edwards et al. (2012). Thus, depending on the nature of the dataset used for the allometric equations, modelers can delineate the application domain and determine to what extent a particular model has local or universal use. We also argue that the proposed method offers a straightforward way to quantify the contribution of the error associated with specific allometric specifications of ecophysiological parameters to the model predictions. For example, our Monte Carlo analysis was founded upon the probability distributions presented in Fig. 4, which reflected the parametric (and/or structural) uncertainty surrounding the maximum phosphorus uptake rates for a given cell morphology (e.g., cell volume, surface-to-volume).

On a final note, interspecific competition patterns and structural shifts in algal assemblages are also determined by factors that are hardly related the allometric approach proposed. For example, there are phytoplankton species that can regulate their buoyancy in a wide range of habitats based on different mechanisms, such as collapse of gas vesicles under rising turgor pressure, regulation of cell growth relative to gas-vesicle production rates that induces changes in buoyancy, and accumulation of photosynthetically fixed carbon in the form of glycogen, acting as a "ballast" that adds to the excess cell density (Kromkamp and Walsby, 1990). Further, colonial and filamentous algal cell formations demonstrate complicated nutrient uptake kinetics that differ significantly from those typically characterizing spherical cells. Upon nitrogen limitation, cyanobacteria show the ability to differentiate between oxygenic photosynthesis (in vegetative cells) and N_2 fixation (in the non-photosynthetic heterocysts (Zehr, 2011). Other distinctive characteristics of cyanobacteria, include toxin production and allelopathic interactions with higher trophic organisms and/or other competing algal functional groups (Grover et al., 2012). In this regard, mathematical submodels have been developed to represent many of these adaptive strategies and support short-term species-specific forecasts. The proposed allometric configuration is not intended to replace the latter constructs but rather to facilitate their integration into management-oriented models without over-inflating their complexity. Namely, we believe that the linkage between biological rates and cell morphology allows building parsimonious model that can partly explain the phytoplankton variability, while any extra complexity should be geared toward the mechanistic understanding of site-specific management problems (e.g., *Microcystis* blooms).

In his "Critique for Ecology", Peters (1991) concluded that "…The theories of predictive ecology tend to be empirical, because only empiricism allows realistic estimates of the uncertainty associated with unconsidered factors, holistic and simplistic because complex or mechanistic theories seem inapplicable, and practical, because the theories are often inspired by pressing questions about nature rather than the scholasticisms of academia…" In this study, although we do not agree with Peters' skepticism about the value of mechanistic explanation, we do believe that the integration of process-based and empirical models offers an appealing prospect from both methodological and ecophysiological point of view. We propose the development of modeling frameworks that are based on our best mechanistic understanding of plankton processes and ecosystem feedback loops, yet remain within the bounds of data-based parameter estimation and therefore can accommodate rigorous error analysis. Size structure of algal communities is an important regulatory factor of the biogeochemical fluxes and

energy transfer via the aquatic food webs that ultimately affects system productivity. The improvement of empirical description of plankton model parameters could reconcile the ongoing debate on the need to balance between simplicity and realism (Anderson, 2005; Arhonditsis, 2010; Flynn, 2005).

Acknowledgments

This project has received funding from the Krembil Foundation. Additional financial support was provided by the National Sciences and Engineering Research Council of Canada (NSERC) through a Doctoral Graduate Scholarship (Yuko Shimoda).

Appendix A. Supplementary data

Supplementary data to this article can be found online at http://dx.doi.org/10.1016/j.ecoinf.2015.11.001.

References

Aksnes, D., Egge, J., 1991. A theoretical model for nutrient uptake in phytoplankton. Mar. Ecol. Prog. Ser. 70, 65–72.
Anderson, T.R., 2005. Plankton functional type modeling: running before we can walk? J. Plankton Res. 27, 1073–1081.
Anderson, D., Lively, J., Reardon, E., Price, C., 1985. Sinking characteristics of dinoflagellate cysts. Limnol. Oceanogr. 30, 1000–1009.
Arhonditsis, G.B., 2010. Useless arithmetic? Lessons learnt from aquatic biogeochemical modeling. In: Hanrahan, G. (Ed.), Modeling of Pollutants in Complex Environmental Systems. ILM Publications, Hertfordshire, UK (512 pp.).
Arhonditsis, G.B., Brett, M.T., 2004. Evaluation of the current state of mechanistic aquatic biogeochemical modeling. Mar. Ecol. Prog. Ser. 271, 13–26.
Arhonditsis, G.B., Brett, M.T., 2005. Eutrophication model for Lake Washington (USA) Part I. Model description and sensitivity analysis. Ecol. Model. 187, 140–178.
Arhonditsis, G.B., Stow, C.A., Steinberg, L.J., Kenney, M.A., Lathrop, R.C., McBride, S.J., Reckhow, K.H., 2006. Exploring ecological patterns with structural equation modeling and Bayesian analysis. Ecol. Model. 192, 385–409.
Arhonditsis, G.B., Paerl, H.W., Valdes-Weaver, L.M., Stow, C.A., Steinberg, L.J., Reckhow, K.H., 2007a. Application of Bayesian structural equation modeling for examining phytoplankton dynamics in the Neuse River Estuary (North Carolina, USA). Estuar. Coast. Shelf Sci. 72, 63–80.
Arhonditsis, G.B., Qian, S.S., Stow, C.A., Lamon, E.C., Reckhow, K.H., 2007b. Eutrophication risk assessment using Bayesian calibration of process-based models: application to a mesotrophic lake. Ecol. Model. 208, 215–229.
Banse, K., 1982. Cell volumes, maximal growth rates of unicellular algae and ciliates, and the role of ciliates in the marine pelagial. Limnol. Oceanogr. 27, 1059–1071.
Barica, J., 1989. Unique limnological phenomena affecting water quality of Hamilton Harbor, Lake Ontario. J. Great Lakes Res. 15, 519–530.
Beven, K., 2006. A manifesto for the equifinality thesis. J. Hydrol. 320, 18–36.
Cavender-Bares, K.K., Rinaldo, A., Chisholm, S.W., 2001. Microbial size spectra from natural and nutrient enriched ecosystems. Limnol. Oceanogr. 46, 778–789.
Cerco, C., Cole, T., 1993. 3-Dimensional eutrophication model of Chesapeake Bay. J. Environ. Eng. ASCE 119, 1006–1025.
Chambers, P., Kalff, J., 1985. Depth distribution and biomass of submersed aquatic macrophyte communities in relation to secchi depth. Can. J. Fish. Aquat. Sci. 42, 701–709.
Charlton, M.N., 2001. The Hamilton Harbour remedial action plan: eutrophication. Verh. Int. Ver. Theor. Angew. Limnol. 27, 4069–4072.
Chen, C.S., Ji, R.B., Schwab, D.J., Beletsky, D., Fahnenstiel, G.L., Jiang, M.S., Johengen, T.H., Vanderploeg, H., Eadie, B., Budd, J.W., Bundy, M.H., Gardner, W., Cotner, J., Lavrentyev, P.J., 2002. A model study of the coupled biological and physical dynamics in Lake Michigan. Ecol. Model. 152, 145–168.
Chen, S., Fath, B.D., Chen, B., 2011. Information-based network environ analysis: a system perspective for ecological risk assessment. Ecol. Indic. 11, 1664–1672.
Costanza, R., Sklar, F., 1985. Articulation, accuracy and effectiveness of mathematical-models — a review of fresh-water wetland applications. Ecol. Model. 27, 45–68.
Cottingham, K.L., Carpenter, S.R., 1998. Population, community, and ecosystem variates as ecological indicators: phytoplankton responses to whole-lake enrichment. Ecol. Appl. 8, 508–530.
Cottingham, K.L., Schindler, D.E., 2000. Effects of grazer community structure on phytoplankton response to nutrient pulses. Ecology 81, 183–200.
Cottingham, K.L., Glaholt, S., Brown, A.C., 2004. Zooplankton community structure affects how phytoplankton respond to nutrient pulses. Ecology 85, 158–171.
Cyr, H., Pace, M., 1993. Allometric theory — extrapolations from individuals to communities. Ecology 74, 1234–1245.
Denman, K.L., 2003. Modeling planktonic ecosystems: parameterizing complexity. Prog. Oceanogr. 57, 429–452.
Dermott, R.M., 2007. Assessment Of Lower Food Web In Hamilton Harbour, Lake Ontario, 2002–2004. Great Lakes Laboratory for Fisheries and Aquatic Sciences, Burlington, Ont.
Downing, J.A., Rigler, F.H., 1984. A Manual On Methods For The Assessment Of Secondary Productivity In Fresh Waters. 2 Sub edition. Blackwell Science Inc., Oxford; Boston: St. Louis, Mo.
Edwards, K.F., Thomas, M.K., Klausmeier, C.A., Litchman, E., 2012. Allometric scaling and taxonomic variation in nutrient utilization traits and maximum growth rate of phytoplankton. Limnol. Oceanogr. 57, 554–566.
Elliott, J.A., Irish, A.E., Reynolds, C.S., Tett, P., 2000. Modeling freshwater phytoplankton communities: an exercise in validation. Ecol. Model. 128, 19–26.
Elliott, J.A., Reynolds, C.S., Irish, A.E., 2001. An investigation of dominance in phytoplankton using the PROTECH model. Freshw. Biol. 46, 99–108.
Fennel, W., 2008. Towards bridging biogeochemical and fish-production models. J. Mar. Syst. 71, 171–194.
Flynn, K.J., 2005. Castles built on sand: dysfunctionality in plankton models and the inadequacy of dialogue between biologists and modellers. J. Plankton Res. 27, 1205–1210.
Friebele, E., Correll, D., Faust, M., 1978. Relationship between phytoplankton cell-size and rate of orthophosphate uptake — in situ observations of an estuarine population. Mar. Biol. 45, 39–52.
Fujiki, T., Taguchi, S., 2002. Variability in chlorophyll alpha specific absorption coefficient in marine phytoplankton as a function of cell size and irradiance. J. Plankton Res. 24, 859–874.
Gin, K.Y.H., Guo, J.H., Cheong, H.F., 1998. A size-based ecosystem model for pelagic waters. Ecol. Model. 112, 53–72.
Grover, J., 1989. Influence of cell shape and size on algal competitive ability. J. Phycol. 25, 402–405.
Grover, J., 1991. Resource competition in a variable environment — phytoplankton growing according to the variable-internal-stores model. Am. Nat. 138, 811–835.
Grover, J.P., Roelke, D.L., Brooks, B.W., 2012. Modeling of plankton community dynamics characterized by algal toxicity and allelopathy: a focus on historical *Prymnesium parvum* blooms in a Texas reservoir. Ecol. Model. 227, 147–161.
Gudimov, A., Stremilov, S., Ramin, M., Arhonditsis, G.B., 2010. Eutrophication risk assessment in Hamilton Harbour: system analysis and evaluation of nutrient loading scenarios. J. Great Lakes Res. 36, 520–539.
Gudimov, A., Ramin, M., Labencki, T., Wellen, C., Shelar, M., Shimoda, Y., Boyd, D., Arhonditsis, G.B., 2011. Predicting the response of Hamilton Harbour to the nutrient loading reductions: a modeling analysis of the "ecological unknowns". J. Great Lakes Res. 37, 494–506.
Hamblin, P.F., He, C., 2003. Numerical models of the exchange flows between Hamilton Harbour and Lake Ontario. Can. J. Civ. Eng. 30, 168–180.
Hamilton, D.P., Schladow, S.G., 1997. Prediction of water quality in lakes and reservoirs. Part I—model description. Ecol. Model. 96, 91–110.
Hansen, B., Bjornsen, P., Hansen, P., 1994. The size ratio between planktonic predators and their prey. Limnol. Oceanogr. 39, 395–403.
Hiriart-Baer, V.P., Milne, J., Charlton, M.N., 2009. Water quality trends in Hamilton Harbour: two decades of change in nutrients and chlorophyll a. J. Great Lakes Res. 35, 293–301.
Hudson, R., Morel, F., 1990. Iron transport in marine phytoplankton: kinetics of cellular and medium coordination reactions. Limnol. Oceanogr. 35, 1002–1020.
Huisman, J., Weissing, F.J., 1999. Biodiversity of plankton by species oscillations and chaos. Nature 402, 407–410.
Hurtt, G.C., Armstrong, R.A., 1996. A pelagic ecosystem model calibrated with BATS data. Deep-Sea Res. II Top. Stud. Oceanogr. 43, 653–683.
Hyenstrand, P., Rydin, E., Gunnerhed, M., Linder, J., Blomqvist, P., 2001. Response of the cyanobacterium *Gloeotrichia echinulata* to iron and boron additions — an experiment from Lake Erken. Freshw. Biol. 46, 735–741.
Johnk, K.D., Huisman, J., Sharples, J., Sommeijer, B., Visser, P.M., Stroom, J.M., 2008. Summer heatwaves promote blooms of harmful cyanobacteria. Glob. Chang. Biol. 14, 495–512.
Jorgensen, S.E., Padisak, J., 1996. Does the intermediate disturbance hypothesis comply with thermodynamics? Hydrobiologia 323, 9–21.
Jorgensen, S.E., Nielsen, S.N., Jorgensen, L.A., 1991. Handbook Of Ecological Parameters And Ecotoxicology. Pergamon Press, Amsterdam.
Kerimoglu, O., Straile, D., Peeters, F., 2012. Role of phytoplankton cell size on the competition for nutrients and light in incompletely mixed systems. J. Theor. Biol. 300, 330–343.
Kim, D.-K., Zhang, W., Hiriart-Baer, V., Wellen, C., Long, T., Boyd, D., Arhonditsis, G.B., 2014. Towards the development of integrated modeling systems in aquatic biogeochemistry: a Bayesian approach. J. Great Lakes Res. 40, 73–87.
Klapwijk, A., Snodgrass, W., 1985. Model for lake-bay exchange flow. J. Great Lakes Res. 11, 43–52.
Kromkamp, J., Walsby, A., 1990. A computer-model of buoyancy and vertical migration in cyanobacteria. J. Plankton Res. 12, 161–183.
Kruk, C., Huszar, V.L.M., Peeters, E.T.H.M., Bonilla, S., Costa, L., Lurling, M., Reynolds, C.S., Scheffer, M., 2010. A morphological classification capturing functional variation in phytoplankton. Freshw. Biol. 55, 614–627.
Le Quere, C., 2006. Reply to Horizons Article "Plankton functional type modeling: running before we can walk" Anderson (2005): I. Abrupt changes in marine ecosystems? J. Plankton Res. 28, 871–872.
Levin, S., 1992. The problem of pattern and scale in ecology. Ecology 73, 1943–1967.
Li, W.K.W., 2002. Macroecological patterns of phytoplankton in the northwestern North Atlantic Ocean. Nature 419, 154–157.
Litchman, E., Klausmeier, C.A., Schofield, O.M., Falkowski, P.G., 2007. The role of functional traits and trade-offs in structuring phytoplankton communities: scaling from cellular to ecosystem level. Ecol. Lett. 10, 1170–1181.
Litchman, E., Klausmeier, C.A., Yoshiyama, K., 2009. Contrasting size evolution in marine and freshwater diatoms. Proc. Natl. Acad. Sci. U. S. A. 106, 2665–2670.
Loh, P.S., Molot, L.A., Nuernberg, G.K., Watson, S.B., Ginn, B., 2013. Evaluating relationships between sediment chemistry and anoxic phosphorus and iron release across three different water bodies. Inland Waters 3, 105–118.

Marchetti, A., Cassar, N., 2009. Diatom elemental and morphological changes in response to iron limitation: a brief review with potential paleoceanographic applications. Geobiology 7, 419–431.
Mayer, T., Manning, P., 1990. Inorganic contaminants in suspended solids from Hamilton Harbor. J. Great Lakes Res. 16, 299–318.
Menden-Deuer, S., Lessard, E.J., 2000. Carbon to volume relationships for dinoflagellates, diatoms, and other protist plankton. Limnol. Oceanogr. 45, 569–579.
Mieleitner, J., Reichert, P., 2008. Modeling functional groups of phytoplankton in three lakes of different trophic state. Ecol. Model. 211, 279–291.
Moloney, C., Field, J., 1991. The size-based dynamics of plankton food webs I. A simulation model of carbon and nitrogen flows. J. Plankton Res. 13, 1003–1038.
Molot, L.A., Li, G., Findlay, D.L., Watson, S.B., 2010. Iron-mediated suppression of bloom-forming cyanobacteria by oxine in a eutrophic lake. Freshw. Biol. 55, 1102–1117.
Molot, L.A., Watson, S.B., Creed, I.F., Trick, C.G., McCabe, S.K., Verschoor, M.J., Sorichetti, R.J., Powe, C., Venkiteswaran, J.J., Schiff, S.L., 2014. A novel model for cyanobacteria bloom formation: the critical role of anoxia and ferrous iron. Freshw. Biol. 59, 1323–1340.
Moore, J.K., Doney, S.C., Lindsay, K., Mahowald, N., Michaels, A.F., 2006. Nitrogen fixation amplifies the ocean biogeochemical response to decadal timescale variations in mineral dust deposition. Tellus Ser. B Chem. Phys. Meteorol. 58, 560–572.
Mullin, M., Sloan, P., Eppley, R., 1966. Relationship between carbon content cell volume and area in phytoplankton. Limnol. Oceanogr. 11, 307–311.
Munawar, M., Fitzpatrick, M., 2007. An integrated assessment of the microbial and planktonic communities of Hamilton Harbour. Can. Tech. Rep. Fish. Aquat. Sci. 2729, 43–63.
Murphy, T.P., Irvine, K., Guo, J., Davies, J., Murkin, H., Charlton, M., Watson, S.B., 2003. New microcystin concerns in the lower great lakes. Water Qual. Res. J. Can. 38, 127–140.
Nogueira, E., Woods, J.D., Harris, C., Field, A.J., Talbot, S., 2006. Phytoplankton coexistence: results from an individual-based simulation model. Ecol. Model. 198, 1–22.
Omlin, M., Brun, R., Reichert, P., 2001. Biogeochemical model of Lake Zurich: sensitivity, identifiability and uncertainty analysis. Ecol. Model. 141 (1–3), 105–123.
Pahlow, M., Riebesell, U., Wolf-Gladrow, D.A., 1997. Impact of cell shape and chain formation on nutrient acquisition by marine diatoms. Limnol. Oceanogr. 42, 1660–1672.
Perhar, G., Arhonditsis, G.B., Brett, M.T., 2012. Modeling the role of highly unsaturated fatty acids in planktonic food web processes: a mechanistic approach. Environ. Rev. 20, 155–172.
Peters, R.H., 1983. The Ecological Implications Of Body Size. Cambridge University Press, New York.
Peters, R.H., 1991. A Critique For Ecology. Cambridge University Press, New York.
Poulin, F.J., Franks, P.J.S., 2010. Size-structured planktonic ecosystems: constraints, controls and assembly instructions. J. Plankton Res. 32, 1121–1130.
Ramin, M., Stremilov, S., Labencki, T., Gudimov, A., Boyd, D., Arhonditsis, G.B., 2011. Integration of numerical modeling and Bayesian analysis for setting water quality criteria in Hamilton Harbour, Ontario, Canada. Environ. Model. Softw. 26, 337–353.
Ramin, M., Labencki, T., Boyd, D., Trolle, D., Arhonditsis, G.B., 2012. A Bayesian synthesis of predictions from different models for setting water quality criteria. Ecol. Model. 242, 127–145.
Rao, Y.R., Marvin, C.H., Zhao, J., 2009. Application of a numerical model for circulation, temperature and pollutant distribution in Hamilton Harbour. J. Great Lakes Res. 35, 61–73.
Raven, J.A., 1980. Nutrient transport in microalgae. Adv. Microb. Physiol. 21, 47–226.
Ray, S., Berec, L., Straskraba, M., Jorgensen, S.E., 2001. Optimization of exergy and implications of body sizes of phytoplankton and zooplankton in an aquatic ecosystem model. Ecol. Model. 140, 219–234.
Reynolds, C.S., 1984. The Ecology of Freshwater Phytoplankton. Cambridge University Press, Cambridge, UK.
Reynolds, C.S., 2006. The Ecology of Phytoplankton. Cambridge University Press.
Reynolds, C.S., Huszar, V., Kruk, C., Naselli-Flores, L., Melo, S., 2002. Towards a functional classification of the freshwater phytoplankton. J. Plankton Res. 24, 417–428.
Sarmiento, J., Slater, R., Fasham, M., Ducklow, H., Toggweiler, J., Evans, G., 1993. A seasonal three-dimensional ecosystem model of nitrogen cycling in the North-Atlantic Euphotic Zone. Glob. Biogeochem. Cycles 7, 417–450.
Scheffer, M., Rinaldi, S., Huisman, J., Weissing, F.J., 2003. Why plankton communities have no equilibrium: solutions to the paradox. Hydrobiologia 491, 9–18.
Segura, A.M., Kruk, C., Calliari, D., Fort, H., 2013. Use of a morphology-based functional approach to model phytoplankton community succession in a shallow subtropical lake. Freshw. Biol. 58, 504–512.
Serizawa, H., Amemiya, T., Rossberg, A.G., Itoh, K., 2008. Computer simulations of seasonal outbreak and diurnal vertical migration of cyanobacteria. Limnology 9, 185–194.
Shimoda, Y., Arhonditsis, G.B., 2016. Phytoplankton functional type modeling: running before we can walk? A critical evaluation of the current state of knowledge. Ecol. Model. 320, 29–43.
Shimoda, Y., Azim, M.E., Perhar, G., Ramin, M., Kenney, M.A., Sadraddini, S., Gudimov, A., Arhonditsis, G.B., 2011. Our current understanding of lake ecosystem response to climate change: what have we really learned from the north temperate deep lakes? J. Great Lakes Res. 37, 173–193.
Sin, Y., Wetzel, R.L., 2002. Ecosystem modeling analysis of size-structured phytoplankton dynamics in the York River estuary, Virginia (USA). I. Development of a plankton ecosystem model with explicit feedback controls and hydrodynamics. Mar. Ecol. Prog. Ser. 228, 75–90.
Smith, R.E.H., Kalff, J., 1982. Size-dependent phosphorus uptake kinetics and cell quota in phytoplankton. J. Phycol. 18, 275–284.
Sommer, U., 1995. An experimental test of the intermediate disturbance hypothesis using cultures of marine phytoplankton. Limnol. Oceanogr. 40, 1271–1277.
Soranno, P.A., Carpenter, S.R., Lathrop, R.C., 1997. Internal phosphorus loading in Lake Mendota: response to external loads and weather. Can. J. Fish. Aquat. Sci. 54, 1883–1893.
Stolte, W., Riegman, R., 1996. A model approach for size-selective competition of marine phytoplankton for fluctuating nitrate and ammonium. J. Phycol. 32, 732–740.
Tang, E., 1995. The allometry of algal growth rates. J. Plankton Res. 17, 1325–1335.
Thingstad, T.F., Strand, E., Larsen, A., 2010. Stepwise building of plankton functional type (PFT) models: a feasible route to complex models? Prog. Oceanogr. 84, 6–15.
Tian, R.C., Vezina, A.F., Legendre, L., Ingram, R.G., Klein, B., Packard, T., Roy, S., Savenkoff, C., Silverberg, N., Therriault, J.C., Tremblay, J.E., 2000. Effects of pelagic food–web interactions and nutrient remineralization on the biogeochemical cycling of carbon: a modeling approach. Deep-Sea Res. II Top. Stud. Oceanogr. 47, 637–662.
Van Nes, E.H., Scheffer, M., 2005. A strategy to improve the contribution of complex simulation models to ecological theory. Ecol. Model. 185, 153–164.
Watson, S.B., Ridal, J., Boyer, G.L., 2008. Taste and odour and cyanobacterial toxins: impairment, prediction, and management in the Great Lakes. Can. J. Fish. Aquat. Sci. 65, 1779–1796.
Wetzel, R.G., 2001. Limnology: Lake and River Ecosystems. 3rd ed. Academic Press, New York, USA.
Wirtz, K.W., 2013. Mechanistic origins of variability in phytoplankton dynamics: part I: niche formation revealed by a size-based model. Mar. Biol. 160, 2319–2335.
Wirtz, K.W., 2014. A biomechanical and optimality-based derivation of prey-size dependencies in planktonic prey selection and ingestion rates. Mar. Ecol. Prog. Ser. 507, 81–94.
Zehr, J.P., 2011. Nitrogen fixation by marine cyanobacteria. Trends Microbiol. 19, 162–173.
Zhang, W., Arhonditsis, G.B., 2008. Predicting the frequency of water quality standard violations using Bayesian calibration of eutrophication models. J. Great Lakes Res. 34, 698–720.
Zhao, J., Ramin, M., Cheng, V., Arhonditsis, G.B., 2008a. Plankton community patterns across a trophic gradient: the role of zooplankton functional groups. Ecol. Model. 213, 417–436. http://dx.doi.org/10.1016/j.ecolmodel.2008.01.016.
Zhao, J., Ramin, M., Cheng, V., Arhonditsis, G.B., 2008b. Competition patterns among phytoplankton functional groups: how useful are the complex mathematical models? Acta Oecol.-Int. J. Ecol. 33, 324–344.

OPTIMIZING THE COMPLEXITY OF PHYTOPLANKTON FUNCTIONAL GROUP MODELLING: AN ALLOMETRIC APPROACH

(Electronic Supplementary Material)

Yuko Shimoda[1], Yerubandi R. Rao[2], Sue Watson[2], George B. Arhonditsis[1*]

[1]Department of Physical & Environmental Sciences, University of Toronto,
Toronto, Ontario, Canada, M1C 1A4
[2]Environment Canada, Water Science and Technology, National Water Research Institute,
Burlington, Ontario, Canada, L7R 4A6

* Corresponding author
E-mail: georgea@utsc.utoronto.ca, Tel.: +1 416 208 4858; Fax: +1 416 287 7279

FIGURES LEGENDS

Figure S1: Distribution of allometric parameter values corresponding to cell volume (μm^3), as used in our Monte Carlo simulations: (a) maximum growth rate; (b) half saturation constant for ammonium uptake; (c) maximum phosphorous uptake rate; (d) half saturation constant for phosphorous uptake; (e) maximum internal phosphate quota; (f) minimum internal phosphate quota; (g) basal metabolism; (h) settling velocity; (i) light attenuation coefficient for the self-shading effect; (j) algal food quality.

Figure S2: Calibration results of the spatially-explicit Hamilton Harbour model: (a) total chlorophyll a and three functional groups A, B, and C, (b) total zooplankton biomass and two functional groups; herbivorous and omnivorous zooplankton, (c) total phosphorous and (d) phosphate concentration in four segments. Diamond marks represent observed mean value with vertical error bars representing the 95% uncertainty intervals.

Figure S3: Calibration results of the spatially-explicit Hamilton Harbour model: (a) total nitrogen, (b) ammonium, and (c) nitrate concentration in four segments. Diamond marks represent observed mean value with vertical error bars representing the 95% uncertainty intervals.

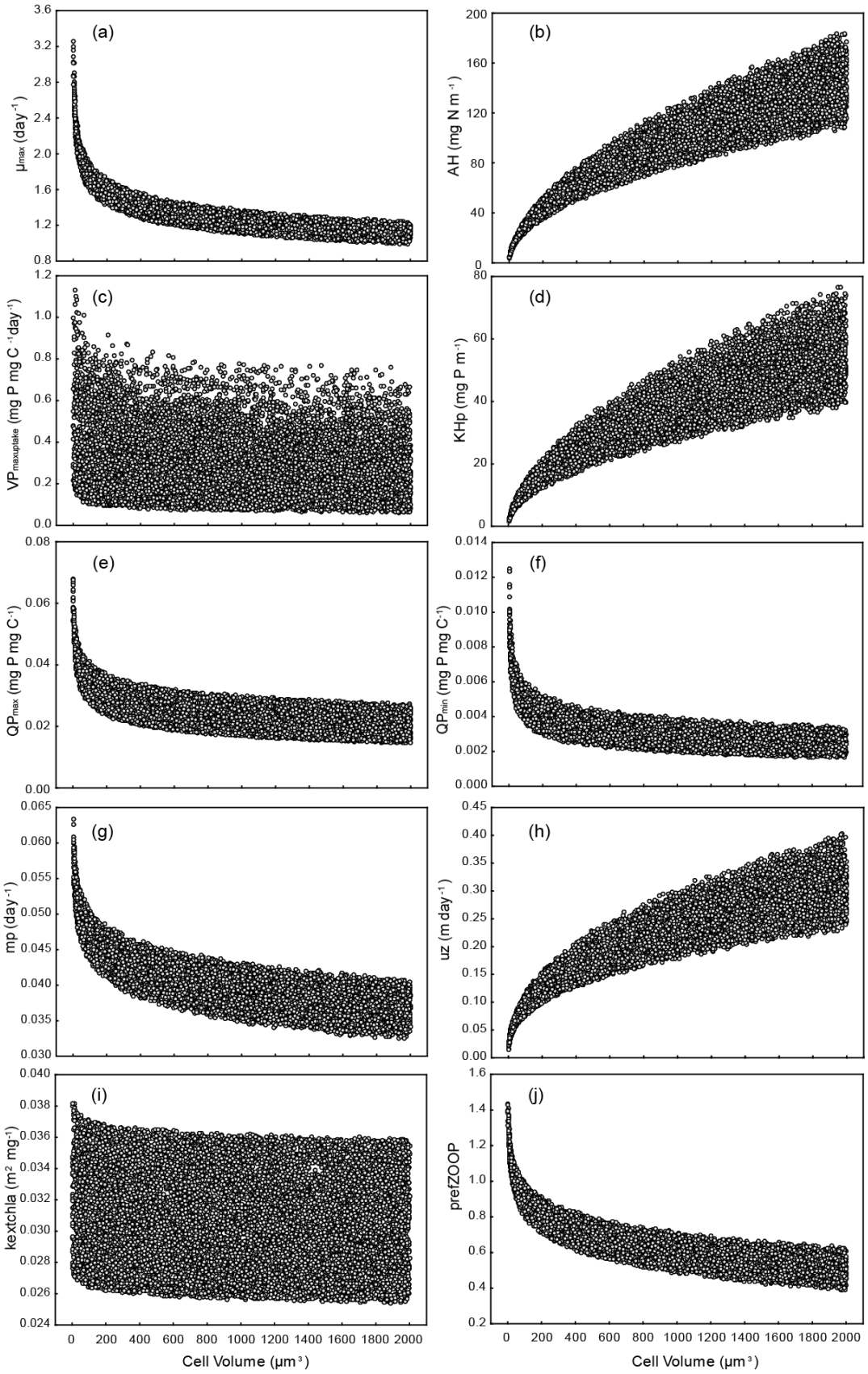
(a)
μmax (day-1)
(b)
AH (mg N m-1)
(c)
VPmaxuptake (mg P mg C -1day-1)
(d)
KHp (mg P m-1)
(e)
QPmax (mg P mg C-1)
(f)
QPmin (mg P mg C-1)
(g)
mp (day-1)
(h)
uz (m day-1)
(i)
kextchla (m2 mg-1)
(j)
prefZOOP
Cell Volume (μm3)
Cell Volume (μm3)

Figure S1

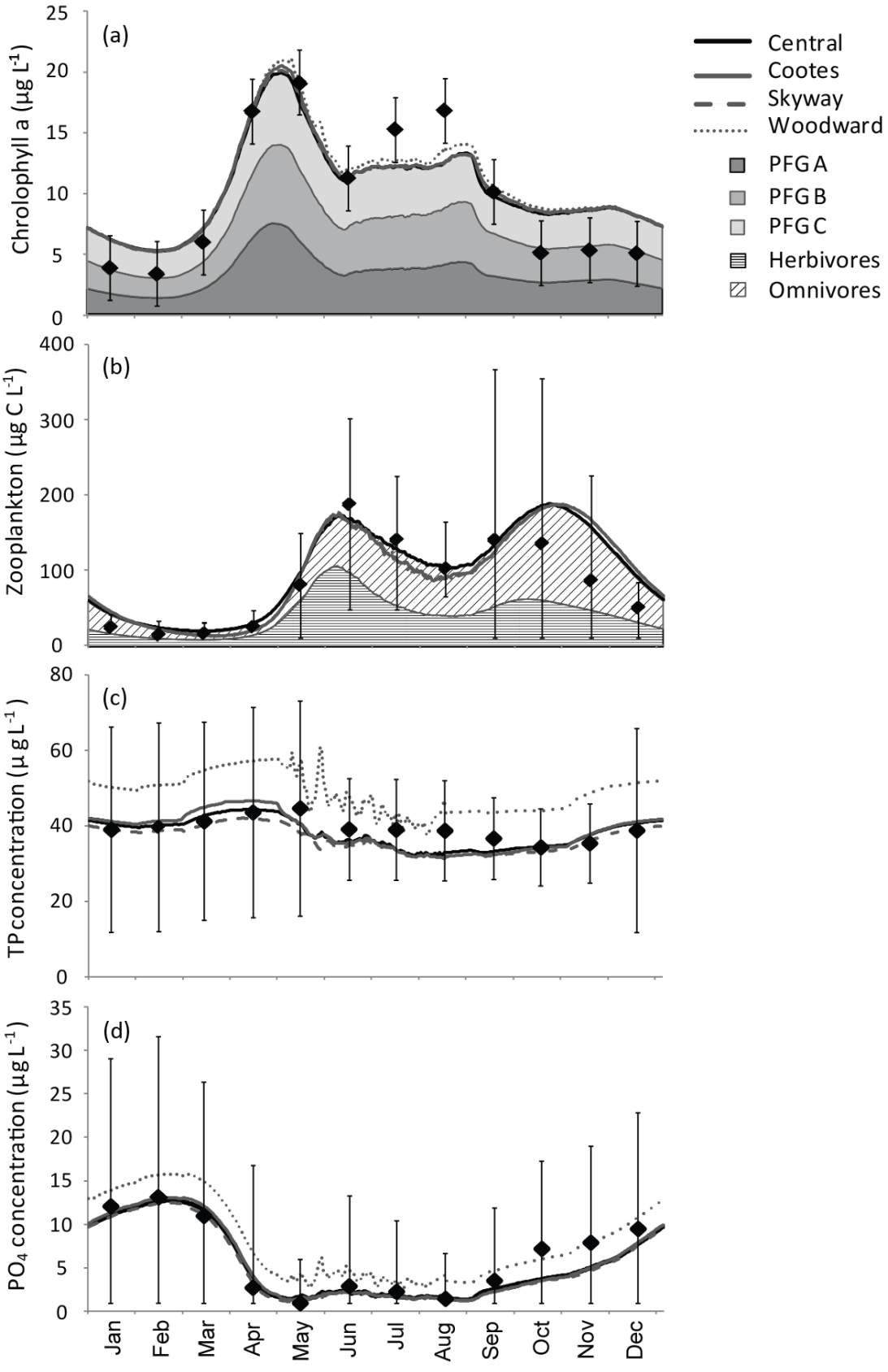
(a)
Chrolophyll a (µg L-1)
25
20
15
10
5
0
Central
Cootes
Skyway
Woodward
PFG A
PFG B
PFG C
Herbivores
Omnivores
(b)
Zooplankton (µg C L-1)
400
300
200
100
0
(c)
TP concentration (µ g L-1)
80
60
40
20
0
(d)
PO4 concentration (µg L-1)
35
30
25
20
15
10
5
0
Jan
Feb
Mar
Apr
May
Jun
Jul
Aug
Sep
Oct
Nov
Dec
Month

Figure S2

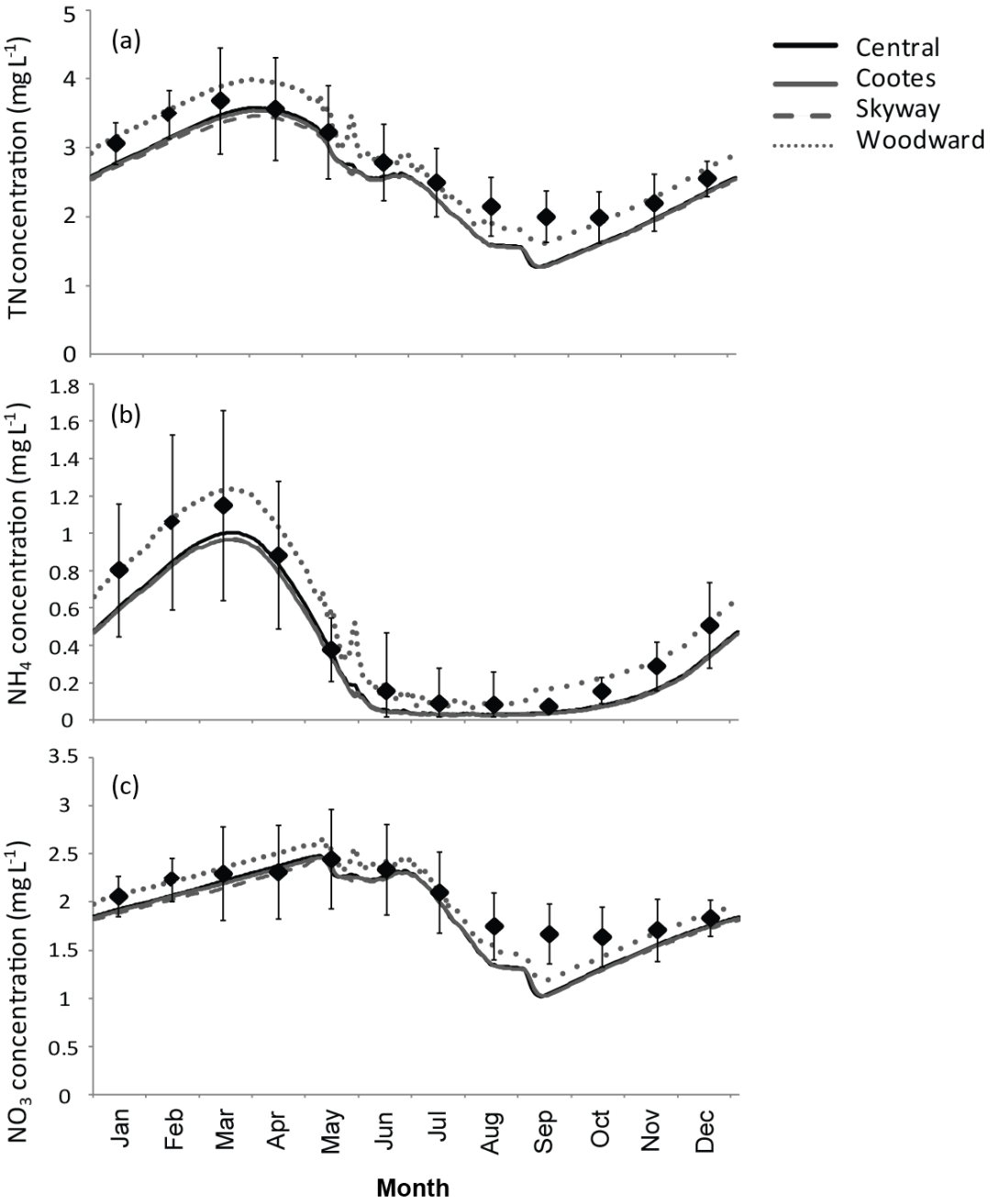
(a)
(b)
(c)
TN concentration (mg L-1)
NH4 concentration (mg L-1)
NO3 concentration (mg L-1)
Central
Cootes
Skyway
Woodward
Jan
Feb
Mar
Apr
May
Jun
Jul
Aug
Sep
Oct
Nov
Dec
Month

Figure S3

Table S1: Mathematical description of the model. The *i* subscript refers to the phytoplankton groups *PFG A, PFG B, PFG C;* the *j* subscript refers to herbivorous and omnivorous zooplankton*;* the *x* subscript refers to the spatial segments epilimnion, mesolimnion and hypolimnion.

No.	State Variable	Term	Equation
1	**Phytoplankton biomass**	$\frac{dPHYT_{i,x}}{dt}$	$=growth_{i,x} \times PHYT_{i,x} - mp_i \times e^{kt(Tx-Tempref)} \times PHYT_{i,x} - uz_i \times PHYT_{i,x}/z_x - filter_i \times e^{ktfilt(Tx-Tempref)} \times PHYT_{i,x} - Grazing_{herb\ i,x} \times ftemperature_{herb\ x} \times ZOOP_{herb\ x} - Grazing_{omni\ i,x} \times ftemperature_{omni\ x} \times ZOOP_{omni\ x} \pm Exchanges_{PHYT\ i\ Vertical} \pm Exchanges_{PHYT\ i\ Lake\ Ontario}$, *where*
	Growth rate	$growth_{i,x}$	$= \mu_{max\ i} \times fnutrient_{i,x} \times flight_{i,x} \times ftemperature_{i,x}$
	Nutrient limitation	$fnutrient_{i,x}$	$=min\{\varphi NA_{i,x}, \varphi PO_{4i,x}\}$
	Nitrogen limitation	$\varphi NA_{i,x}$	$=\varphi NO_{3i,x} + \varphi NH_{4i,x}$
	Nitrate limitation	$\varphi NO3_{i,x}$	$= (NO_{3x}\, e^{(-\psi i \cdot NH4_x)})/(NO_{3x} + NH_i)$
	Ammonium limitation	$\varphi NH4_{i,x}$	$=NH_{4x}/(NH_{4x}+AH_i)$
	Phosphate limitation	$\varphi PO4_{i,x}$	$= (Pint_{i,x} - QPmin_i)/(QPmax_i - QPmin_i)$
	Intracellular phosphorus content	$\frac{dPint_{i,x}}{dt}$	$=Pup_{i,x} \times Pfb_{i,x} - growth_{i,x} \times Pint_{i,x}$
	Phosphorus uptake	$Pup_{i,x}$	$=VP_{maxuptake\ i} \times (PO_{4x}/(PO_{4x} + KHp_i))$
	Feedback control	$Pfb_{i,x}$	$= (QPmax_i - Pint_{i,x})/(QPmax_i - QPmin_i)$
	Light limitation	$flight_{i,x}$	$=2.718 \times (FD/(kext_x \times z_x))(e^{-a1} - e^{-a0})$, *where* $a0_i = (I/Ik_i)e^{-kext_x \times H_x}$, $a1_i = (I/Ik_i)e^{-kext_x (z_x + H_x)}$
	Light attenuation	$kext_x$	$=Kextchla_i \sum_i PHYT_{i,x} \times ChlaC_i + Kextb$
	Temperature limitation	$ftemperature_{i,x}$	$= e^{(-KTgr_i (T_x - Topt_i)^2)}$
		FD	$=$*the fractional day length* $(0 \le FD \le 1)$
2	**Herbivorous zooplankton biomass**	$\frac{dZOOP_{herb,x}}{dt}$	$=[\sum_i Grazing_{herb\ i,x} \times ftemperature_{herb,x} \times asfood_{herb,i} + Grazing_{herbdet,x} \times ftemperature_{herb,x} \times asfood_{herb,det}] \times ZOOP_{herb,x} - mz_{herb} \times e^{kt(Tx-Tempref)} \times ZOOP_{herb,x} - Grazing_{omniherb,x} \times ftemperature_{omni,x} \times ZOOP_{omni,x} \pm Exchanges_{herb\ Vertical} \pm Exchanges_{herb\ Lake\ Ontario}$
	Grazing rate for phytoplankton	$Grazing_{herb\ i,x}$	$=maxgrazing_{herb} \times (prefZOOP_{i,x} \times PHYT_{i,x}) / (KZ_{herb} + Food_{herb,x})$
	Grazing rate for detritus	$Grazing_{herbdet,x}$	$=maxgrazing_{herb} \times (pref_{herbdet,x} \times Detritus_x) / (KZ_{herb} + Food_{herb,x})$
	Grazing rate by omnivorous zooplankton	$Grazing_{omniherb,x}$	$=maxgrazing_{omni} \times (pref_{omniherb,x} \times ZOOP_{herb,x}) / (KZ_{omni} + Food_{omni,x})$
	Abundance of food in layer *x*	$Food_{herb,x}$	$=\sum_i pref_{herb\ i,x} \times PHYT_{i,x} + pref_{herbdet,x} \times Detritus_x$
	Preference of zooplankton for phytoplankton *i*	$pref_{herb\ i,x}$	$(prefZOOPf_{herb,i} \times PHYT_{i,x}) / (\sum_i prefZOOP_i \times PHYT_{i,x} + pref_{herbdet} \times Detritus_x)$
	Preference of zooplankton for detritus	$pref_{herbdet,x}$	$= (pref_{herbdet} \times Detritus_x) / (\sum_i prefZOOP_{herb,i} \times PHYT_{i,x} + pref_{herbdet} \times Detritus_x)$

No.	State Variable	Term	Equation
	Temperature limitation for growth	$ftemperature_{herb,x}$	$= e^{(-KTgr_{herb}(T_x - Topt_{herb})^2)}$
3	**Omnivorouszooplankton biomass**	$\frac{dZOOP_{omni,x}}{dt}$	$=[\sum_i Grazing_{omni\ i,x} \times ftemperature_{omni,x} \times asfood_{omni,i} + Grazing_{omnidet,x} \times ftemperature_{omni,x} \times asfood_{omnidet} + Grazing_{omniherb,x} \times ftemperature_{omni,x} \times asfood_{omniherb}] \times ZOOP_{omni,x} - mz_{omni} \times e^{kt(Tx-Tempref)} \times ZOOP_{omni,x} \pm Exchanges_{omni\ Vertical} \pm Exchanges_{omni\ Lake\ Ontario}$
	Grazing rate for phytoplankton	$Grazing_{omni\ i,x}$	$=maxgrazing_{omni} \times (prefZOOP_{i,x} \times PHYT_{i,x}) / (KZ_{omni} + Food_{omni,x})$
	Grazing rate for herbivorous zooplankton	$Grazing_{omniherb,x}$	$=maxgrazing_{omni} \times (prefZOOP_{herb,x)} \times PHYT_{herb,x}) / (KZ_{omni} + Food_{omni,x})$
	Grazing rate for detritus	$Grazing_{omnidet,x}$	$=maxgrazing_{omni} \times (pref_{omnidet,x} \times Detritus_x) / (KZ_{omni} + Food_{omni,x})$
	Abundance of food in layer *x*	$Food_{omni,x}$	$=\sum_i prefZOOP_i \times PHYT_{i,x} + pref_{omnidet,x} \times Detritus_x$
	Preference of omnivorous zooplankton for phytoplankton *i*	$Pref_{omni\ i,x}$	$= (prefZOOP_{,i} \times PHYT_{i,x}) / (\sum_i prefZOOP_i \times PHYT_{i,x} + pref_{omnidet} \times Detritus_x)$
	Preference of zooplankton for detritus	$Pref_{omnidet,x}$	$= (pref_{omnidet} \times Detritus_x) / (\sum_i prefZOOP_i \times PHYT_{i,x} + pref_{omnidet} \times Detritus_x)$
	Temperature limitation for growth	$ftemperature_{omni,x}$	$= e^{(-KTgr_{omni}(T_x - Topt_{omni})^2)}$
4	**Detritus concentration**	$\frac{dDetritus_x}{dt}$	$=\sum_i [(1 - \alpha_{DOC\ i}) \times mp_i \times e^{kt(Tx-Tempref)} \times PHYT_{i,x}] + \sum_{j=omni,herbi} [(1 - \alpha_{DOC_j}) \times mz_j \times e^{kt(Tx-Tempref)} \times ZOOP_{j,x}] - [(maxgrazing_{herb} \times pref_{herbdet,x} \times Detritus_x) / (KZ_{herb} + Food_{herb,x})] \times ftemperature_{herb,x} \times ZOOP_{herb,x} - [(maxgrazing_{omni} \times pref_{omnidet,x} \times Detritus_x) / (KZ_{omni} + Food_{omni,x})] \times ftemperature_{omni,x} \times ZOOP_{omni,x} - uz_{(biogenic)} \times Detritus_x / z_x - KCmineral_x \times Detritus_x$
	Carbon mineralization rate	$KCmineral_x$	$= ftemperature\_min_x \times KCrefmineral$; *where*
	Temperature limitation for mineralization	$ftemperature\_min_x$	$= e^{(-KTFmin(T_x - Toptmin)^2)}$
5	**Phosphate concentration**	$\frac{dPO_{4x}}{dt}$	$= -\sum_i Pup_{i,x} \times Pfb_{i,x} \times PHYT_{i,x} + \sum_i \alpha_{PO4\ i} \times mp_i \times e^{kt(Tx-Tempref)} \times Pint_{i,x} \times PHYT_{i,x} + \sum_{j=herbi,omni} \alpha_{PO4\ j} \times mz_j \times e^{kt(Tx-Tempref)} \times PC_j \times ZOOP_{j,x} + KPmineral_x \times OP_x - FePrecipitation \pm ExchangesPO_{4Vertical} \pm ExchangesPO_{4Lake\ Ontario} + PO_4EXOG_{EPI} + PO_4ENDOG_x$, *where*
	Phosphorus mineralization rate	$KPmineral_x$	$= ftemperature\_min_x \times KPrefmineral$; *where*
	Iron-induced	$FePrecipitation$	$= (1-(9.4 \times [Fe_{Steel\ Mills} + 1400]^{-0.31})) \times PO_{4\,x}$

No.	State Variable	Term	Equation
	precipitation due to Steel Mills discharge		
6	**Organic phosphorus concentration**	$\frac{dOP_x}{dt}$	$= DetritusP_x - \sum_{j=omni,herbi} DetritusGrazing\ P_{j,x} \times ftemperature_{j,x} \times ZOOP_{j,x} - SettlingP_x \times OP_x / z_x - KPmineral_x \times OP_x \pm ExchangesOP_{Vertical} \pm ExchangesOP_{Lake\ Ontario} + OPEXOG_{EPI} + OPENDOG_x$
	Biogenic organic phosphorus accumulation	$DetritusP_x$	$= \sum_i (1 - \alpha_{PO4\,i}) \times mp_i \times e^{kt(T_x - Tempref)} \times Pint_{i,x} \times PHYT_{i,x} + \sum_{j=omni,herbi} (1 - \alpha_{PO4\,j}) \times mz_j \times e^{kt(T_x - Tempref)} \times PC_j \times ZOOP_{j,x}$
	Loss due to zooplankton grazing upon detritus	$DetritusGrazingP_{j,x}$	$= (maxgrazing_j \times Pref_{det\,j,x} \times DetritusP_x) / (KZ_j + Food_{j,x})$
	Loss due to particulate phosphorus settling	$SettlingP_x$	$= (DetritusP_x / OP_x) \times uz_{(biogenic)} + (1 - (DetritusP_x / OP_x)) \times uz$
7	**Ammonium concentration**	$\frac{dNH_{4x}}{dt}$	$= -\sum_i \varphi NH_{4\,i,x} \times \mu_{max\,i} \times flight_{i,x} \times ftemperature_{i,x} \times N/C_{i,x} \times PHYT_{i,x} + \sum_i \alpha NH_{4\,i} \times mp_i \times e^{kt(Tx - Tempref)} \times N/C_{i,x} \times PHYT_{i,x} + \sum_{j=omni,herbi} aNH4_j \times mz_j \times e^{kt(Tx - Tempref)} \times N/C_j \times ZOOP_{j,x} + KNmineral_x \times ON_x - Nitrification_x \pm ExchangesNH4_{Vertical} \pm Exchanges\ NH4_{Lake\ Ontario} + NH4EXOG_{EPI} + NH4ENDOG_x$
	Mineralization rate	$KNmineral_x$	$= KN_{refmineral} \times ftemperature\_min_x$
	Nitrification rate	$Nitrification_x$	$= Nitrifmax \times flightnitr_x \times (DO_x / (DO_x + KHdonit)) \times (NH4_x / KHnh4nit + NH4_x) \times ftempnitr_x$
	Light limitation	$flightnitr_x$	$= 1$ when $I_x \leq 0.1 \times I$, else $flightnitr_x = 0$
	Temperature limitation	$ftempnitr_x$	$= e^{(-KTFgrnitr(T_x - Toptnitr)^2)}$
	Intensity of light in compartment x	I_x	$= I / (kext_x \times z_x)(e^{-kext_x \times H_x} - e^{-kext_x(z_x + H_x)})$
	Nitrogen-to-carbon ratio of the phytoplankton cells	$N/C_{i,x}$	$= 16 \times Pint_{i,x}$
8	**Nitrate concentration**	$\frac{dNO_{3x}}{dt}$	$= -\sum_i \varphi NO3_{i,x} \times \mu_{max\,i} \times flight_{i,x} \times ftemperature_{i,x} \times N/C_{i,x} \times PHYT_{i,x} + Nitrification_x - Denitrification_x \pm ExchangesNO3_{Vertical} \pm ExchangesNO3_{Lake\ Ontario} + NO3EXOG_{EPI} + NO3ENDOG_x;$
	Denitrification rate	$Denitrification_x$	$= Denitrifmax \times (KHdodenit / (DO_x + KHdodenit)) \times (NO_{3\,x} / KHno3nit + NO_{3\,x}) \times ftempdenitr_x$
	Temperature limitation	$ftempdenitr_x$	$= e^{(-KTgrdenitr(T_x - Toptdenitr)^2)}$

No.	State Variable	Term	Equation
9	**Organic nitrogen concentration**	$\frac{dON_x}{dt}$	$= Detritus\ N_x - \sum_j DetritusGrazing\ N_{j,x} \times ftemperature_{j,x} \times ZOOP_{j,x} -$ $[Detritus\ N_x / ON_x \times Vbiosettling + (1\text{-}Detritus\ N_x / ON_x) \times uz] \times ON_x - KNmineral_x \times ON_x \pm ExchangesON_{Vertical} \pm ExchangesON_{Lake\ Ontario} + ONEXOG_{EPI} + ONENDOG_x$
	Biogenic organic nitrogen accumulation	$Detritus\ N_x$	$= \sum_i (1 - a_{NH4\,i}) \times mp_i \times e^{kt(Tx-Tempref)} \times N/C_{i,x} \times PHYT_{i,x,}$ $+ \sum_j (1 - a_{NH4\,j}) \times mz_j \times e^{kt(Tx-Tempref)} \times N/C_j \times ZOOP_{j,x}$
	Loss due to zooplankton grazing upon detritus	$DetritusGrazingN_{j,x}$	$= maxgrazing_j \times pref_{det\,j,x} \times Detritus\ N_x / (KZ_j + Food_{j,x})$
10	**Sediment submodel**		
10.1	**Phosphate sediment release**	$\frac{dPO_{4sed_x}}{dt}$	$= (1 - \beta_P) \times Pdeposition - (\alpha s_{PO4} \times PO4_{sed\,x} \times e^{Ktsed(Tsedx-Tempref_{sed})})$
	Organic phosphorus sedimentation	$Pdeposition$	$= (\sum_i uz_i \times Pint_{i,x} \times PHYT_{i,x} + SettlingP_x \times OP_x)$
10.2	**Ammonium sediment release**	$\frac{dNH_{4sed_x}}{dt}$	$= (1 - \beta_N) \times Ndeposition - (\alpha s_{NH4} \times NH_{4\,sed\,x} \times e^{Kt}sed^{(Tsed\,x-\,Tempref_{sed})})$ $- Nitrifmax_{sed} \times (DO_x / (DO_x + KHdonit_{sed})) \times$ $\times (NH_{4\,sed\,x} / (KHnh4nit_{sed} + NH_{4\,sed\,x})) \times ftempnitrsed_x$
	Loss due to particulate nitrogen settling	$Ndeposition$	$= \sum_i uz_i \times N/C_{i,x} \times PHYT_{i,x} + uzN_x \times ON_x$, where
	Settling rate of particulate nitrogen	uzN_x	$Detritus\ N_x / ON_x \times uz_{(biogenic)} + (1\text{-}Detritus\ N_x / ON_x) \times uz$
	Temperature limitation for nitrification in the sediments	$ftempnitrsed_x$	$= e^{(-KTgrnitr_{sed}(T_x - Toptnitr_{sed})^2)}$
10.3	**Nitrate sediment release**	$\frac{dNO_{3sed_x}}{dt}$	$= Nitrifmax_{sed} \times (DO_x / (DO_x + KHdonit)) \times (NH_{4sed\,x} / (KHnh4nit + NH_{4sed\,x})) \times ftempnitr_x - (as_{NO3} \times NO3_{sed\,x} \times e^{Ktsed(Tsed}x^{-Tempref}sed^{)}) - Denitrifmax_{sed} \times (KHdodenit_{sed} / (DO_x + KHdodenit_{sed})) \times (NO_{3sed\,x} / KHno3denit_{sed} + NO_{3\,sed\,x}) \times ftempdenitrsed_x$
	Temperature limitation for denitrification in the sediments	$ftempdenitrsed_x$	$= e^{(-KTgrdenitr_{sed}(T_x - Toptdenitr_{sed})^2)}$
	Rate of sediment release of organic nitrogen	$ONSED_x$	$= ONosed \bullet e^{(kt_{sed}(Tsed-Tempref_{sed})}$, where
		$ONosed$	$= OPosed \times TN/TP,$
	Rate of sediment release of organic phosphorus	$OPSED_x$	$= OPosed \bullet e^{(kt_{sed}(Tsed-Tempref_{sed})}$, where
		$OPosed$	$= 0.1\ mg\ m^{-2}\ day^{-1}$
	Total nitrogen to total phosphorus ratio	TN/TP	$= 21$

Table S2: Description and calibration values of model parameters

Symbol	*Description*	*Values*	*Units*	*Sources*
AH_{PFGA}	Half saturation constant for ammonium uptake by PFG A	100	mg N m^{-3}	
AH_{PFGB}	Half saturation constant for ammonium uptake by PFG B	80	mg N m^{-3}	
AH_{PFGC}	Half saturation constant for ammonium uptake by PFG C	60	mg N m^{-3}	
$\alpha_{DOC\ herbi}$	Fraction of herbivorous zooplankton mortality becoming dissolved organic carbon	0.5	-	9
$\alpha_{DOC\ omni}$	Fraction of omnivorous zooplankton mortality becoming dissolved organic carbon	0.5	-	9
$\alpha_{DOC\ PFGA}$	Fraction of PFG A mortality becoming dissolved organic carbon	0.5	-	9
$\alpha_{DOC\ PFGB}$	Fraction of PFG B mortality becoming dissolved organic carbon	0.5	-	9
$\alpha_{DOC\ PFGC}$	Fraction of PFG C mortality becoming dissolved organic carbon	0.5	-	9
$\alpha_{NH4\ herbi}$	Fraction of herbivorous zooplankton mortality becoming ammonium	0.5	-	9
$\alpha_{NH4\ omni}$	Fraction of omnivorous zooplankton mortality becoming ammonium	0.5	-	9
$\alpha_{NH4\ PFGA}$	Fraction of PFG A mortality becoming ammonium	0.5	-	9
$\alpha_{NH4\ PFGB}$	Fraction of PFG B mortality becoming ammonium	0.5	-	9
$\alpha_{NH4\ PFGC}$	Fraction of PFG C mortality becoming ammonium	0.5	-	9
αs_{NO3}	Sediment nitrate release rate	0.5	day^{-1}	
as_{NH4}	Sediment ammonium release rate	0.5	day^{-1}	
αs_{PO4}	Sediment phosphate release rate	0.5	day^{-1}	
$\alpha_{PO4\ herbi}$	Fraction of herbivorous zooplankton mortality becoming phosphate	0.8	-	9
$\alpha_{PO4\ omni}$	Fraction of omnivorous zooplankton mortality becoming phosphate	0.8	-	9
$\alpha_{PO4\ PFGA}$	Fraction of PFG A mortality becoming phosphate	0.25	-	9
$\alpha_{PO4\ PFGB}$	Fraction of PFG B mortality becoming phosphate	0.25	-	9
$\alpha_{PO4\ PFGC}$	Fraction of PFG C mortality becoming phosphate	0.25	-	9
$asfood_{herbi\ det}$	Herbivorous zooplankton assimilation efficiency for detritus	0.45	-	
$asfood_{herbi\ PFGA}$	Herbivorous zooplankton assimilation efficiency for PFG A	0.5	-	
$asfood_{herbi\ PFGB}$	Herbivorous zooplankton assimilation efficiency for PFG B	0.5	-	
$asfood_{herbi\ PFGC}$	Herbivorous zooplankton assimilation efficiency for PFG C	0.15	-	
$asfood_{omni\ det}$	Omnivorous zooplankton assimilation efficiency for detritus	0.45	-	
$asfood_{omni\ herb}$	Omnivorous zooplankton assimilation efficiency for herbivorous zooplankton	0.55	-	
$asfood_{omni\ PFGA}$	Omnivorous zooplankton assimilation efficiency for PFG A	0.5	-	

No.	State Variable	Term	Equation		
	$asfood_{omni\ PFGB}$	Omnivorous zooplankton assimilation efficiency for PFG B	0.5	-	
	$asfood_{omni\ PFGC}$	Omnivorous zooplankton assimilation efficiency for PFG C	0.15	-	
	$ChlaC_{PFGA}$	Chlorophyll to carbon ratio in PFG A	0.02	-	2,8,10,14
	$ChlaC_{PFGB}$	Chlorophyll to carbon ratio in PFG B	0.02	-	2, 8, 10,14
	$ChlaC_{PFGC}$	Chlorophyll to carbon ratio in PFG C	0.02	-	2, 8, 10,14
	$Denitrifmax$	Maximum denitrification rate	5	mg N m^{-2} day^{-1}	
	$Denitrifmax_{sed}$	Maximum sediment denitrification rate	25	mg N m^{-2} day^{-1}	
	$filter_{PFGA}$	PFG A filtering rate from dreissenids	0.02	day^{-1}	
	$filter_{PFGB}$	PFG B filtering rate from dreissenids	0.015	day^{-1}	
	$filter_{PFGC}$	PFG C filtering rate from dreissenids	0.01	day^{-1}	
	$\mu_{max\ PFGA}$	Maximum growth for PFG A	Table 1	day^{-1}	
	$\mu_{maxPFGB}$	Maximum growth for PFG B	Table 1	day^{-1}	
	$\mu_{maxPFGC}$	Maximum growth for PFG C	Table 1	day^{-1}	
	$H_{epilimnion}$	Distance from water surface to top of the epilimnion segment layer	0	m	
	$H_{metalimnion}$	Distance from water surface to top of the metalimnion segment	8	m	
	$H_{hypolimnion}$	Distance from water surface to top of the hypolimnion segment	16	m	
	Ik_{PFGA}	Half saturation light intensity for PFG A	150	MJ m^{-2} day^{-1}	
	Ik_{PFGB}	Half saturation light intensity for PFG B	150	MJ m^{-2} day^{-1}	
	Ik_{PFGC}	Half saturation light intensity for PFG C	150	MJ m^{-2} day^{-1}	
	$KCrefmineral$	Particulate carbon mineralization rate at reference temperature	0.01	day^{-1}	
	$Kextb$	Background light attenuation	0.15	m^{-1}	14
	$Kextchla_{PFGA}$	Light attenuation coefficient for PFG A	Table 1	m^2 mg^{-1}	12,14
	$Kextchla_{PFGB}$	Light attenuation coefficient for PFG B	Table 1	m^2 mg^{-1}	12,14
	$Kextchla_{PFGC}$	Light attenuation coefficient for PFG C	Table 1	m^2 mg^{-1}	12,14
	$KHdodenit$	Half saturation concentration of DO deficit required for nitrification	0.5	mg O_2 m^{-3}	9
	$KHdodenit_{sed}$	Half saturation concentration of DO deficit required for denitrification in the sediments	1	mg O_2 m^{-3}	
	$KHdonit$	Half saturation concentration of DO required for nitrification	1	mg O_2 m^{-3}	9
	$KHdonit_{sed}$	Half saturation concentration of DO required for nitrification in the sediments	2	mg O_2 m^{-3}	
	$KHnh4nit$	Half saturation concentration of ammonium required for nitrification	1	mg N m^{-3}	9
	$KHnh4nit_{sed}$	Half saturation concentration of ammonium required for nitrification in the sediments	75	mg N m^{-3}	
	$KHno3denit$	Half saturation concentration of nitrate required for denitrification	15	mg N m^{-3}	9
	$KHno3denit_{sed}$	Half saturation concentration of DO deficit required for denitrification in the sediments	15	mg O_2 m^{-3}	
	KHp_{PFGA}	Half saturation constant for phosphorus uptake by PFG A	Table 1	mg P m^{-3}	
	KHp_{PFGB}	Half saturation constant for phosphorus uptake by PFG B	Table 1	mg P m^{-3}	

No.	State Variable	Term	Equation		
KHp_{PFGC}		Half saturation constant for phosphorus uptake by PFG C	Table 1	mg P m^{-3}	
KNrefmineral		Nitrogen mineralization rate at reference temperature	0.01	day^{-1}	9, 14
KPrefmineral		Phosphorus mineralization rate at reference temperature	0.005	day^{-1}	3, 14, 9
kt		Effects of temperature on phytoplankton mortality	0.069	$^oC^{-1}$	3, 7,9,10
ktfilt		Effects of temperature on phytoplankton filtration	0.069	$^oC^{-1}$	
KTFmin		Effects of temperature on mineralization	0.004	$^oC^{-2}$	
KTgrdenitr		Effect of temperature on denitrification	0.004	$^oC^{-2}$	
$KTgrdenitr_{sed}$		Effect of temperature on sediment denitrification	0.004	$^oC^{-2}$	
$KTgr_{herbi}$		Effect of temperature on herbivorous zooplankton	0.005	$^oC^{-2}$	1-5
KTgrnitr		Effect of temperature on nitrification	0.004	$^oC^{-2}$	9,15
$KTgrnitr_{sed}$		Effect of temperature on sediment nitrification	0.004	$^oC^{-2}$	
$KTgr_{omni}$		Effect of temperature on omnivorous zooplankton	0.005	$^oC^{-2}$	2,3
$KTgr_{PFGA}$		Effect of temperature on PFG A	0.005	$^oC^{-2}$	3, 9,12,13
$KTgr_{PFGB}$		Effect of temperature on PFG B	0.005	$^oC^{-2}$	3, 9,12,13
$KTgr_{PFGC}$		Effect of temperature on PFG C	0.005	$^oC^{-2}$	3, 9,12,13
kt_{sed}		Effects of temperature on sedimentation	0.004	-	
KZ_{herb}		Half saturation constant for grazing by herbivorous zooplankton	105	mg C m^{-3}	6-7
KZ_{omni}		Half saturation constant for grazing by omnivorous zooplankton	105	mg C m^{-3}	6,7
$maxgrazing_{herb}$		Maximum grazing rate for herbivorous zooplankton	0.5	day^{-1}	6-7
$maxgrazing_{omni}$		Maximum grazing rate for omnivorous zooplankton	0.5	day^{-1}	6,8
mp_{PFGA}		Basal metabolism for PFG A	Table 1	day^{-1}	
mp_{PFGB}		Basal metabolism for PFG B	Table 1	day^{-1}	
mp_{PFGC}		Basal metabolism for PFG C	Table 1	day^{-1}	
mz_{herb}		Mortality rate for herbivorous zooplankton	0.15	day^{-1}	1-3, 6,7,8
mz_{omni}		Mortality rate for omnivorous zooplankton	0.17	day^{-1}	1-3, 6-8
N/C_{herbi}		Nitrogen to carbon ratio for omnivorous zooplankton	0.2	mg N mg C^{-1}	16,17
N/C_{omni}		Nitrogen to carbon ratio for herbivorous zooplankton	0.2	mg N mg C^{-1}	16,17
NH_{PFGA}		Half saturation constant for nitrate uptake by PFG A	Table 1	mg N m^{-3}	12-14
NH_{PFGB}		Half saturation constant for nitrate uptake by PFG B	Table 1	mg N m^{-3}	12-14
NH_{PFGC}		Half saturation constant for nitrate uptake by PFG C	Table 1	mg N m^{-3}	12-14

No.	State Variable	Term	Equation		
Nitrifmax		Maximum nitrification rate at optimal temperature	20	mg N m^{-3} day^{-1}	9, 14,15
$Nitrifmax_{sed}$		Maximum sediment nitrification rate	50	mg N m^{-2} day^{-1}	
P/C_{herbi}		Phosphorus to carbon ratio for herbivorous zooplankton	0.025	mg P mg C^{-1}	16,17
P/C_{omni}		Phosphorus to carbon ratio for omnivorous zooplankton	0.025	mg P mg C^{-1}	16,17
$pref_{herb\ det}$		Preference of herbivorous zooplankton for detritus	1	-	
$pref_{omnidet}$		Preference of omnivorous zooplankton for detritus	1	-	
$pref_{omniherb}$		Preference of omnivorous zooplankton for herbivorous zooplankton	1.5	-	
$prefZOOP_{PFG\ A}$		Preference of zooplankton (both herbivore and omnivore) for PFG A	Table 1	-	
$prefZOOP_{PFG\ B}$		Preference of zooplankton (both herbivore and omnivore) for PFG B	Table 1	-	
$prefZOOP_{PFG\ C}$		Preference of zooplankton (both herbivore and omnivore) for PFG C	Table 1	-	
$QP_{maxPFGA}$		Maximum PFG A internal phosphate quota	Table 1	mg P mg C^{-1}	
$QP_{maxPFGB}$		Maximum PFG B internal phosphate quota	Table 1	mg P mg C^{-1}	
$QP_{maxPFGC}$		Maximum PFG C internal phosphate quota	Table 1	mg P mg C^{-1}	
$QP_{minPFGA}$		Minimum PFG A internal phosphorus quota	Table 1	mg P mg C^{-1}	
$QP_{minPFGB}$		Minimum PFG B internal phosphorus quota	Table 1	mg P mg C^{-1}	
$QP_{minPFGC}$		Minimum PFG C internal phosphorus quota	Table 1	mg P mg C^{-1}	
Tempref		Water reference temperature	20	^{o}C	3,7, 9,10
$Tempref_{sed}$		Sediment reference temperature	20	^{o}C	
Toptdenitr		Optimal temperature for denitrification	20	^{o}C	
$Toptdenitr_{sed}$		Optimal temperature for denitrification in sediment	20	^{o}C	
$Topt_{herbi}$		Reference temperature for herbivorous zooplankton	20	^{o}C	1-5
Toptmin		Optimal temperature for mineralization	20	^{o}C	
Toptnitr		Optimal temperature for nitrification	20	^{o}C	9,15
$Toptnitr_{sed}$		Optimal temperature for denitrification in sediment	20	^{o}C	
$Topt_{omni}$		Optimal temperature for omnivorous zooplankton	20	^{o}C	1-5
$Topt_{PFGA}$		Optimal temperature for PFG A growth	20	^{o}C	3,7, 9,10
$Topt_{PFGB}$		Optimal temperature for PFG B growth	22	^{o}C	3,7, 9,10
$Topt_{PFGC}$		Optimal temperature for PFG C growth	24	^{o}C	3,7, 9,10
$uz_{(biogenic)}$		Biogenic particle settling velocity	0.15	m day^{-1}	
uz		Allochthonous particle settling velocity	0.65	m day^{-1}	2, 9,12,13
uz_{PFGA}		PFG A settling velocity	Table 1	m day^{-1}	
uz_{PFGB}		PFG B settling velocity	Table 1	m day^{-1}	
uz_{PFGC}		PFG C settling velocity	Table 1	m day^{-1}	
$VP_{maxuptakePFGA}$		Maximum phosphorus uptake rate for PFG A	Table 1	mg P mg C^{-1} day^{-1}	
$VP_{maxuptakePFGB}$		Maximum phosphorus uptake rate for PFG B	Table 1	mg P mg C^{-1} day^{-1}	

No.	State Variable	Term	Equation	
$VP_{maxuptakePFGC}$		Maximum phosphorus uptake rate for PFG C	Table 1	mg P mg C^{-1} day^{-1}
β_N		Fraction of inert nitrogen buried into deeper sediment	0.4	-
β_P		Fraction of inert phosphorus buried into deeper sediment	0.9	-
ψ_{PFGA}		Strength of the ammonium inhibition for nitrate uptake	0.05	$(\mu g\ N/L)^{-1}$
ψ_{PFGB}		Strength of the ammonium inhibition for nitrate uptake	0.05	$(\mu g\ N/L)^{-1}$
ψ_{PFGC}		Strength of the ammonium inhibition for nitrate uptake	0.045	$(\mu g\ N/L)^{-1}$
$z_{epilimnion}$		Depth of epilimnion department	8	m
$z_{mesolimnion}$		Depth of mesolimnion department	8	m
$z_{hypolimnion}$		Depth hypolimnion department	8	m

1) Lampert and Sommer, 1997; 2) Wetzel, 2001; 3) Omlin et al., 2001b; 4) Orcutt and Porter, 1983; 5) Downing and Rigler, 1984; 6) Sommer, 1989; 7) Jorgensen et al., 1991; 8) Chen et al., 2002(and references therein); 9) Cerco and Cole, 1994(and references therein); 10) Reynolds, 1984; 11) Sandgren, 1991; 12) Arhonditsis and Brett, 2005; 13) Reynolds, 2006; 14) Hamilton and Schladow, 1997 (and references therein); 15) Berounsky and Nixon, 1990; 16) Hessen and Lyche, 1991; 17) Sterner et al., 1992.

References

Arhonditsis, G.B., Brett, M.T., 2005. Eutrophication model for Lake Washington (USA). Part I. Model description and sensitivity analysis. Ecol. Model. 187, 140–178.

Berounsky, V.M., Nixon, S.W., 1990. Temperature and the annual cycle of nitrification in waters of Narragansett Bay. Limnol. Oceanogr. 35, 1610–1617.

Cerco, C., Cole, T., 1993. 3-Dimensional Eutrophication Model of Chesapeake Bay. J. Environ. Eng.-ASCE 119, 1006–1025.

Chen, C.S., Ji, R.B., Schwab, D.J., Beletsky, D., Fahnenstiel, G.L., Jiang, M.S., Johengen, T.H., Vanderploeg, H., Eadie, B., Budd, J.W., Bundy, M.H., Gardner, W., Cotner, J., Lavrentyev, P.J., 2002. A model study of the coupled biological and physical dynamics in Lake Michigan. Ecol. Model. 152, 145–168.

Downing, J.A., Rigler, F.H., 1984. A Manual on Methods for the Assessment of Second Productivity in Fresh Water, second ed. Blackwell Scientific Publications, Oxford, UK.

Hamilton, D.P., Schladow, S.G., 1997. Prediction of water quality in lakes and reservoirs. Part I—Model description. Ecol. Model. 96, 91–110.

Hessen, D.O., Lyche, A., 1991. Interspecific and intraspecific variations in zooplankton element composition. Arch. Hydrobiol. 121, 343–353.

Jorgensen, S.E., Nielsen, S.N., Jorgensen, L.A., 1991. Handbook of ecological parameters and ecotoxicology. Pergamon Press, Amsterdam.

Lampert, W., Sommer, U., 1997. Limnoecology: The Ecology of Lakes and Streams. Oxford University Press.

Omlin, M., Brun, R., Reichert, P., 2001. Biogeochemical model of Lake Zurich: sensitivity, identifiability and uncertainty analysis. Ecol. Model. 141 (1–3), 105–123.

Orcutt, J.D., Porter, K.G., 1983. Diel vertical migration by zooplankton—constant and fluctuating temperature effects on life-history parameters of daphnia. Limnol. Oceanogr. 28 (4), 720–730.

Reynolds, C.S., 2006. The Ecology of Phytoplankton. Cambridge University Press.

Reynolds, C.S., 1984. The Ecology of Freshwater Phytoplankton. Cambridge University Press, Cambridge, UK.

Sandgren, C.D., 1991. Growth and Reproductive Strategies of Freshwater Phytoplankton. Cambridge University Press.

Sommer, U., 1989. Phytoplankton ecology. Succession in Plankton Communities. Springer-Verlag.

Sterner, R.W., Elser, J.J., Hessen, D.O., 1992. Stoichiometric relationships among producers, consumers, and nutrient cycling in pelagic ecosystems. Biogeochemistry 17, 49–67.

Wetzel, R.G., 2001. Limnology: Lake and River Ecosystems, 3rd ed. Academic Press, New York, USA.